# Evaluating microemboli clearance in a mouse model of microinfarction

Fiona Haugen

A thesis submitted to the University of Ottawa in partial fulfillment of the requirements for the Master's degree in Neuroscience

Department of Cellular and Molecular Medicine
Faculty of Medicine
University of Ottawa

*Abstract*

Cerebral microinfarcts, ranging from 100μm to 3mm in diameter, occur as a result of ischemic microvessel occlusion. Microinfarcts have been found to contribute to cognitive decline and are particularly prevalent in dementia patients and the aging population. Microemboli occlusions are primarily cleared via fibrinolysis and hemodynamic forces to re-establish blood flow. Angiophagy, where vessels engulf and expel microemboli, may also mitigate damage caused by micro-occlusions. Previous rodent studies have proposed conflicting timelines on the extent to which this process occurs and fail to extensively quantify angiophagy in clinically relevant populations, including aging and Alzheimer's disease. To further study this process of angiophagy, we induced micro-occlusions in young, aged and AD mice via injection of 20μm microspheres into the carotid artery. In characterizing this model, we found that most microspheres localized to the cortex, yet when accounting for region size, microspheres were more evenly distributed across regions. When quantifying angiophagy in young non-diseased mice, we found that approximately 43% of microspheres have extravasated from the vessel by day 14. This timeline was delayed in aged mice, with only 10% of microspheres extravasated by day 14. Moreover, in young 3xTg Alzheimer's mice, we find the rate of angiophagy is more efficient at day 14 compared to non-transgenic controls, with 47% and 43% of microspheres extravasated, respectively. A similar trend is observed in aged Alzheimer's mice whereby 38% of microspheres extravasated by day 14 in 3xTg mice, compared to only 30% in non-transgenic controls. Taken together, we show that aging impairs the process of angiophagy, while Alzheimer's mice exhibit an increased ability to extravasate microspheres.

*Table of Contents*

*List of Abbreviations*

**MI** – Microinfarct

**AD** – Alzheimer's disease

**CAA** – Cerebral amyloid angiopathy

**MRI** – Magnetic resonance imaging

**BCAS** – Bilateral common carotid artery stenosis

**GFAP** – Glial fibrillary acidic protein

**NOS** – Nitric oxide synthase

**BBB** – Blood brain barrier

**tPA** – Tissue plasminogen activator

**MMP** – Matrix metalloproteinase

**Aβ -** Amyloid β

**NFTs** – Neurofibrillary tangles

**CBF** – Cerebral blood flow

**LOX** – Lysyl oxidase

**3xTg** – Triple transgenic

**APP** – Amyloid precursor protein

**MAPT** – Microtubule-associated protein tau

**PSEN1** – Presenilin 1

**NTG** – Non-transgenic

**AQP-4** – Aquaporin-4

**MCAO** – middle cerebral artery occlusion

**BACE** – β-site amyloid precursor protein cleaving enzyme

**CCA** – Common carotid artery

**EB** – Evans blue

**ANOVA** – Analysis of variance

**SEM** – Standard error of mean

*List of figures*



*Tables*

*Acknowledgements*

I would like to extend my gratitude to my supervisor, Greg Silasi, who provided invaluable feedback throughout this process. Thank you for this opportunity and helping me learn the ins and outs of the research world.

Thank you to my thesis advisory committee, Dr. Baptiste Lacoste and Dr. Katey Rayner, for their feedback and guidance throughout this process.

Moreover, I would like to thank all the lab members who made my time in the Silasi Lab enjoyable and memorable: Beatriz Romero Quineche, Ségolène Chevallier Rufigny, Shafik Algharbi, Patrick Chary, Sierra Darryl Hedges, and Barman Loghmani. Thank you for all your encouragement, the lovely lunches, and our unforgettable trivia battles.

Thank you to my friends and family, namely my mom and dad, for supporting me throughout this journey and believing in me, I truly could not have done this without you. And thank you to my cat who always kept me company while working on my thesis.

Lastly, thank you to the mice we have sacrificed for the betterment of science.

# *1 Introduction*

## *1.1 Cerebral microinfarcts*

Ischemic occlusion of small cerebral vessels, typically penetrating arterioles, results in the formation of microinfarcts (MIs), which range from 100$\mu$m to 3mm in size[1]. It is hypothesized that MIs accumulate overtime and that the detection of just a few microinfarcts in a post-mortem autopsy are representative of hundreds to thousands brain wide, as merely 0.01% of the brain is sampled in post-mortem tissue studies[1]. MIs are typically undetected by conventional MRIs, however diffusion-weighted imaging and high-resolution structural MRIs can help visualize 1-2mm MIs[1,2]. Although seemingly insignificant, MIs can contribute to cognitive decline and are most common among the aging population[1]. MIs are found in approximately 62% of patients with vascular dementia, 43% of patients with Alzheimer's disease (AD), and in 24% of individuals 75 years or older[3]. Notably, AD patients with microinfarcts have more severe cognitive impairments than AD patients without microinfarcts, however the severity of AD pathology is not correlated with incidence of MIs[4,5].

### *1.1.1 Pathology of cerebral microinfarcts*

The appearance of microinfarcts in human tissue varies, including barrel-shaped, wedge-shaped, triangular, round or stellate[6]. They are typically described as regions of neuronal loss and demyelination, sometimes with cavitation[6,7]. Immune response is observed at the site of infarction, commonly activated macrophages, astrocytes, microglia and white blood cells[6]. The microinfarct core has been found to be infiltrated with CD68-positive macrophages, while GFAP-positive astrocytes are present in the core and extend to the periphery[7]. Notably, chronic microinfarcts exhibit microvascular meshwork in the core and periphery which contain a high density of string vessels – remnants of capillaries lacking endothelial cells with no blood flow[7,8].

### *1.1.2 Distributions of cerebral microinfarcts*

Microinfarcts are found brain-wide, with no definitive conclusions as to whether they manifest with preference to either cortical or subcortical structures[6]. Within the cortex, MIs were found to be most prevalent in the occipital and parietal lobe[9]. One study found that the location of MIs correlated with relating vascular risk factor. Upon examination of 1000 brains post-mortem, it was found cortical MIs were associated with cerebral amyloid angiopathy (CAA),

while subcortical MIs were associated with hypertension, atherosclerosis and arteriosclerosis[10,11]. Moreover, an additional study with 80 samples concluded that MIs in the occipital lobe of the cerebrum were associated with local CAA[12].

*1.2 Cause and risk factors of cerebral microinfarcts*

Several vascular risk factors have been linked to the occurrence of microinfarcts. A study sampling from memory clinic patients found microinfarcts to be associated with intracranial stenosis[13]. Moreover, microinfarcts appear to be a predictor for incidence of major stroke in the future[14]. One study found MIs nearly doubled the risk of subsequent stroke when compared to those without silent MIs[14]. These patients notably had higher systolic/diastolic blood pressures, greater internal and common carotid wall thickness, and incidences of atrial fibrillation, when compared to patients with MIs and no subsequent stroke, or those without MIs[14]. Since microinfarcts often go undetected in conventional MRIs and may be asymptomatic, it is likely these patients have co-existing risk factors that are left untreated and thus result in a major symptomatic stroke later on.

Beyond cerebral risk factors like CAA or presence of macroscopic ischemic infarcts, other factors can influence the prevalence of MIs. In a diffusion-weighted imaging study, 14% of patients undergoing a carotid endarterectomy, a surgical procedure to remove fatty build up on vessel walls, displayed microinfarcts[15]. Additionally, atrial fibrillation, coronary artery disease, and other cardiac disease biomarkers relate to the presence of MIs[13,15-16]. Some studies indicate no relation between hypertension or diabetes and MIs, whereas other studies did observe a positive correlation[16-19].

*1.3 Cerebral microinfarcts and cognitive function*

Microinfarcts are known to be associated with impairment in cognitive function in humans[1]. In one clinical-pathology study sampling post-mortem brains, it was found individuals with more microinfarcts had a greater risk of dementia and MIs were associated with overall lower levels of cognition, including perceptual speed, semantic memory, and episodic memory, even when controlling for age, sex, education, presence of macroinfarcts, AD pathology and Lewis bodies[20]. Moreover, this study found that dementia was related to only multiple MIs, while decreased levels of perceptual speed and semantic memory were associated with both single and multiple MIs[20]. Further, this study found that cortical MIs were associated with poorer

cognitive function, but not subcortical MIs[20]. However, it remains largely unclear the relationship between the location of MIs and their impact on cognitive impairment.

### *1.4 Rodent models of cerebral microinfarction*

Microinfarcts in the human population are often co-morbid with other diseases, such as hypertension or CAA[1]. This makes it difficult to determine the extent to which microinfarcts affect cognition and brain tissue integrity. Mouse models are commonly used to study microinfarcts and associated burden as rodent microvasculature present similarities to that of humans[21]. Microinfarct models focus on the occlusion of penetrating arterioles, typically between 10 and 20um in mice, so as to replicate clinical findings[22]. Rodent models of microinfarcts are either induced or spontaneous.

#### *1.4.1 Microinfarct pathology in rodents*

Microinfarcts in rodent tissue present similarities to the tissue damage observed in humans, such as ischemia and secondary immune response[21]. Microinfarcts are typically described by loss of neuronal tissue, as identified with a lack of NeuN staining or positive for Fluoro-jade staining[21,23]. One study found that occlusion of a single penetrating arteriole forms a columnar infarction over the course of 7 days, and the volume of the infarction correlated with the pre-occlusion flux of red blood cells through the vessel, with greater flux leading to larger microinfarcts[21]. Hypoxia develops in the acute stage, 6-hours post-vessel occlusion, as identified by hypoxyprobe staining[21]. Moreover, the microinfarct core presented with increased alpha-3-nitrotyrosine labelling, representing oxidative protein damage within cells and vasculature[21]. Damaged cells along the border of the microinfarct were propidium iodide-positive, representing a disruption to cell membranes[21]. Immune response following vessel occlusion is notable, typically in the acute stage: macrophages were present in the core and spanned to the periphery, comparable to the immune response observed in post-mortem tissue of humans; activated microglia were also present at the microinfarct border, likely to limit damage; and proliferation of reactive astrocytes was observed[7,21].

#### *1.4.2 Single vessel occlusion*

Occlusion of single penetrating arterioles are commonly performed by activating circulating photosensitive dye, such as Rose Bengal, through a cranial window with a focused

laser[24,25]. Upon photo-activation of the dye, the vessel lining is damaged and platelet aggregation occurs forming blood clots that occlude the vessel and lead to ischemic injury[26]. This technique allows for precise targeting of cortical surface vessels and results in cylindrical-shaped microinfarcts as a result of localized ischemia[24]. Single vessel occlusions can also be induced using a multiphoton absorption-based photothermolysis method. Here, a near infrared femtosecond laser beam is focused to generate multiphoton absorption at the target, without the need of exogenous photosensitive dye[27].

*1.4.3 Diffuse vessel occlusion*

Intra-carotid injections of microemboli can be used to stochastically induce microvessel occlusions across the brain. The occluding microemboli can be cholesterol crystals/fibrin clots or fluorescent microspheres[26]. Although comparable to emboli found in humans, cholesterol crystals and fibrin clots are typically difficult to visualize in histology and can vary in size, whereas microspheres are easily visualized with fluorescent microscopy and are uniform in size[26]. Several studies have investigated the distribution of microspheres in this model, with a majority distributed to the neocortex, followed by the thalamus, or the hippocampus in one case[23,29-33]. Not all lodged microspheres result in the formation of a microinfarct, with one study finding the hippocampus and white matter had the greatest percent of lodged microspheres resulting in injury, as determined by Fluoro-Jade staining, potentially as a result of decreased regional vascularization[23]. Cortical microinfarcts were found to be wedge or column-shaped, resembling what is typically observed in human brain tissue, while microinfarcts observed in other cerebral regions exhibited varying shapes and sizes[31].

*1.4.4 Bilateral Carotid Artery Stenosis*

Bilateral carotid artery stenosis (BCAS) induces hypoperfusion in rodents resulting in the spontaneous formation of subcortical microinfarcts after long-term BCAS (6 months)[34]. This study found that vascular-related changes associated with BCAS were primarily observed in subcortical regions, including an increase in collagen IV density and a decrease in claudin-5 expression, and GFAP expression significantly increased at the 6-month time point compared to shams. Moreover, BCAS can be applied in other mouse models with pathology that increases susceptibility to microinfarcts, namely the Tg-SwDI mouse model exhibiting CAA, which otherwise do not develop microinfarcts, and atherosclerotic ApoE knockout mice[35,36].

*1.4.5 Other models*

Spontaneous microinfarcts have also been observed in other mouse models including endothelial NOS (important for vascular tone and blood pressure maintenance) deficient mice, Notch3 (player in vascular development and mural cell-endothelial communication) mutant mice, and Towne's model of sickle cell[28].

*1.4.6 Neuropathological changes in rodents following diffuse vessel occlusion*

Several studies have characterized the vascular and neuronal changes in rodents following induction of multiple microinfarcts. Commonly, blood brain barrier (BBB) disruption and immune cell response are studied, as these are common features in a post-stroke brain[37].

The van der Wijk group out of the Netherlands have published several papers using a polystyrene microsphere model in rats. In their first paper investigating this microinfarct model, 27,500 microspheres (15um in diameter) were injected which resulted in transient BBB leakage (measured by IgG immunofluorescence) present significantly at day 1 in the experimental hemisphere[38]. Moreover, an immune response in the experimental hemisphere was observed. GFAP signal was used to measure reactive astrocytes and was present significantly at day 1 post-surgery. Iba1 signal was used to measure reactive microglia and was present significantly in the cortex at day 7 and 28 post-surgery. Additionally, this study assessed potential vascular changes in the experimental hemisphere and found there was no difference in the number or length of branches or vessel diameter. However, there was an observable decrease in capillary blood flow in the cortex, striatum, and hippocampus, likely as a result of non-perfusion in these capillaries. They noted capillary nonperfusion was only temporary and blood flow returned at day 7.

In 2020, this same group assessed similar measures in a mixed-microsphere model, injecting approximately 25,000 15um, 5500 25um and 625 50um microspheres together[39]. In this experimental design, BBB leakage was also found to be transient, diminishing at day 7 on a brain-wide scale. Moreover, they observed IgG leakage adjacent to sites of microvessel occlusion. A midline shift was observed, whereby the experimental hemisphere expanded, suggestive of edema in this model. GFAP and Iba1 staining were also assessed, with GFAP signal significantly greater in the experimental hemisphere across all time points (day 1, 3, and 7) and Iba1 signal significantly greater at day 3 and 7. Here, they also observed a shift from ameboid microglia to ramified, indicating immune cell activation.

In 2021, the same concoction of microspheres was used, but infarction (absence of NeuN staining), ischemia (absence of lectin staining), and hypoxia (positive hypoxyprobe staining) were assessed[40]. In the experimental hemisphere, it was found that the number and volume of infarcted regions did not significantly differ across the measured timepoints (day 1, 3 and 7). Conversely, ischemia and hypoxia were shown to decrease significantly overtime, with values nearing zero at day 7, suggestive of successful reperfusion and recovery of hypoxic tissue at risk.

Most recently, in a 2023 study, the van der Wijk group wanted to further investigate if these measures differed depending on the size of microspheres[41]. In three experimental groups, with either 15um, 25um or 50um microspheres, infarction, ischemia and hypoxia were measured as in the previous studies. They found no significant difference in the percent of infarcted regions, non-perfused vessels or hypoxic tissue across all groups. However, there was an increase in the volume of ischemia and infarcted tissue in the 50um microsphere group, and hypoxia in the 25um group, suggesting that the size of the microspheres may result in varying degrees of damage as different sized vessels are targeted. Lastly, BBB leakage was found to be greatest in the 15um microsphere group compared to the 50um group. Additionally, it was shown that IgG intensity was lower in the corpus callosum (white matter) when compared to the cortex (grey matter) and the striatum (white and grey matter), which they suggest is a result of reduced vascular density in white matter.

Overall, these papers identify transient blood brain barrier breakdown, immune response (as measured by reactive astrocytes and microglia), ischemia and hypoxia within the experimental hemisphere as commonly observed cerebral disruptions following MIs.

*1.5 Mechanisms of clearance*

Although small, cerebral microvessels play an important role in oxygen and nutrient delivery through blood-tissue exchange. Subsequently, it is evident that microvessel occlusions result in extensive damage, both locally at the site of blockage, such as hypoxia and subsequent tissue infarction, as well as globally in models of diffuse vessel occlusion, such as blood brain barrier leakage and immune response[38-41]. Thus, repair mechanisms have evolved to protect the brain from subsequent damaged caused by microvessel occlusion.

### *1.5.1 Fibrinolysis and Washout*

Mechanisms are in place to rescue perfusion, whereby lodged intravascular emboli are commonly cleared out via hemodynamic washout or chemical breakdown via thrombolysis[42]. Clearance via washout occurs when cerebral circulation aids in dislodging emboli thus preventing detrimental occlusions. However, the microvasculature is particularly susceptible to microemboli occlusion as a result of small diameter and low-flow velocity[42]. Clearance via chemical breakdown occurs when tissue plasminogen activator (tPA) breaks down clots into smaller fragments that are less likely to become lodged in circulation[43]. tPA activates plasminogen via proteolytic cleavage to convert it to plasmin, the enzyme responsible for breaking down fibrin clots[44].

These clearance mechanisms are not always effective. For example, hemodynamic clearance is often impaired in areas of hypoperfusion whereby the reduced blood flow makes it difficult to wash emboli downstream and some clots are not susceptible to fibrinolysis, such as atheromatous plaques or cholesterol crystals[47,49]. Moreover, one study found that following the injection of cholesterol crystals or fibrin clots, emboli washout and degradation primarily occurred within the first 6 hours post-emboli delivery, beyond which these clearance systems become significantly less efficient[49]. Thus, there is evidently a need for a clearance mechanism beyond this acute timescale.

### *1.5.2 Angiophagy*

First shown by Lam et al., there appears to be a third method of emboli clearance by means of vessel remodeling that functions beyond this acute timepoint[50]. Known as angiophagy, small cerebral vessels (less than 60mM in diameter) engulf occluding emboli and translocate them out of the vessel into the surrounding parenchyma, thus promoting the re-establishment of blood flow[50]. Although the exact mechanism of angiophagy is still unknown, Lam et al. noted that endothelial projections engulf occluding emboli for translocation and heightened levels of gelatinolytic activity detected at sites of vessel occlusion compared to unoccluded vessels[49]. Moreover, addition of a MMP2/9 inhibitor, SB-3CT, decreased clot and microsphere extravasation[50]. Initial signs of angiophagy (lamellipodia projections) have been shown to initiate as early as 3 hours post-emboli delivery[49]. Grutzendler et al. proposed that this process occurs in two distinct phases: (1) retention of the occluding emboli via lamellipodia projections and (2)

extravasation of the emboli outside the vessel into the surrounding parenchyma[49]. It is likely this first stage of angiophagy impairs the alternative clearance mechanisms by preventing emboli washout and insulating the emboli from fibrinolytic agents, thus preventing degradation. The physical translocation of the emboli occurs after 2-7 days[50].

Several studies have investigated the timeline of angiophagy and have presented varying conclusions. This first study in 2010 by Lam et al. primarily used cholesterol and fibrin clots (8-20um) to investigate angiophagy[49]. They found that by day 7, approximately 78% and 58% of the fibrin and cholesterol clots, respectively, had extravasated from the vessel[49]. Although representative of emboli seen in human brain samples, a potential drawback of using fibrin clots is that they are often broken down into smaller fragments, which could potentially be extravasated at different rates than larger emboli.

The van Der Wijk group published a study in 2019 investigating angiophagy in rats using 15um polystyrene microspheres[38]. Here they showed that by day 7, 76% of microspheres had extravasated from the vessels and by day 28, 100% of the microspheres were outside of the vessel[38]. This same group went on to publish a study in 2020 investigating potential differences in the rate of angiophagy depending on the size of the injected emboli[39]. Using 15um and 25um polystyrene microspheres, they argued that the rate of angiophagy was 33% and 18%, respectively, in rats at the day 7 timepoint[39]. Lastly, in another angiophagy study from 2023, van der Wijk used approximately 12um in diameter microspheres composed of poly(ether ester urethane) multiblock copolymer in combination with lactide, glycolide, e-caprolactone, dioxanone and polyethylene glycol with differing makeups[45]. Here it was found that the composition of the microspheres affected the rate of angiophagy, and by day 14, 3.3-20.7% of the microspheres had extravasated, dependent on their makeup[45].

van der Wijk et al. noted that BBB integrity improves at the day 7 timepoint, which is synonymous to the point at which the majority of microspheres had extravasated[38,39]. It is possible the BBB leakage is a result of ischemic insult and the process of vessel reperfusion following angiophagy aids in restoring BBB integrity. Moreover, microglia activation primarily occurred beyond day 3, the timepoint in which microspheres begin to translocate into the parenchyma[38,39]. This is possibly caused by the presence of a foreign body in the brain tissue, signaling for the recruitment of immune cells. Lam et al. showed *in vivo* the engulfment of extravasated fibrin clots by activated phagocytic microglia in a fibrin clot injected model[49].

Lam et al. also investigated angiophagy in aged mice, although to a limited extent, reporting the extravasation rate of microspheres at day 14 to be markedly delayed in aged mice by approximately 35%[50]. The authors suggest that age-related cerebrovascular changes may explain these observations, such as increased basal lamina thickness and collagen deposition[50].

### *1.6 Vascular changes in aging and disease and increase incidence of microinfarcts*

#### *1.6.1 Vascular changes in aging*

Throughout aging, several changes to our brain occur including a decrease in brain size, a decline in cognitive abilities, and vascular differences[52]. Notably, arterial stiffening occurs as we see a decreased expression of arterial elastin[53]. This can result in hypertension as the vessels have a decreased ability to accommodate changes in blood flow. Other vascular changes are observed in aging that contribute to blood brain barrier disruption, such as loss of tight junctions, decreased number of endothelial cells, increased thickness of basement membrane, and sustained inflammation[54]. As well, it is known that fibrinolytic activity decreases with aging[55]. It is hypothesized that these vascular changes occurring with aging, like thickening of basal lamina and increased collagen deposits, may delay the process of angiophagy as the vessels may be less plastic and able to remodel. Collectively, these observations among the elderly may account for the increased prevalence of MIs in this population.

#### *1.6.2 Vascular changes in Alzheimer's disease*

Alzheimer's disease is characterized by the deposition of amyloid β (Aβ) plaques and neurofibrillary tangles (NFTs) composed of hyperphosphorylated tau[56]. It was initially thought that the key pathological determiner of AD is the accumulation of Aβ plaques. However, it appears that Aβ and NFTs are not the only contributors to cognitive impairments in AD patients, as cognitively normal individuals exhibit these pathologies and therapies targeting Aβ accumulation do not entirely rescue AD-related cognitive impairments[56]. The vascular hypothesis of AD has been proposed, arguing that vascular changes seen in AD, commonly preceding cognitive impairments and amyloid β accumulation, drive AD symptoms[56-58]. It has been found that individuals with vascular risk factors, such as atherosclerosis, hypertension, and obesity, are at a greater risk of developing AD[57]. Several vascular changes are observed in AD including hypoperfusion, a decrease in vessel density (likely a result of decreased levels of

angiogenic growth factors), thickened basement membranes (as a result of accumulation of extracellular matrix proteins), and arterial stiffening[57]. In microvasculature, string vessels, tortuous vessels (potentially as a result of decreased elastin), and vessel fragmentation are observed[58]. With cortical microvasculature, the most severe pathologic changes are observed only in regions with neuronal loss[59,60].

Cerebral hypoperfusion is commonly seen in AD patients and precedes other pathological features of the disease, such as hypometabolism and neurodegeneration[61]. Changes in cortical blood flow can be observed years prior to the onset of preclinical symptoms arise[62,63]. Hypoperfusion is detrimental as it disrupts delivery of oxygen and glucose to brain tissue, further exacerbating cognitive deficits[61]. A reduction in cerebral blood flow further exacerbates AD by decreasing the efficiency of Aβ clearance, which subsequently allows for the accumulation of Aβ plaques[35]. In AD patients, hypoxia, commonly as a result of hypoperfusion, has been shown to increase levels of Aβ in the vasculature[57]. Together, hypoperfusion and subsequent hypoxia further exacerbate vessel integrity and the degenerative nature of the disease[57].

One cause of a reduction in CBF is CAA, the accumulation of Aβ plaques in vessel walls, commonly in leptomeningeal and cortical arteries and arterioles[64]. Although a common pathological hallmark of AD, CAA is not limited to individuals with AD[64]. Amyloid angiopathy also occurs in the normal aging population, with 30% of individuals over 60 years old exhibiting this pathology[49]. AD and CAA together is seen in approximately 81-98% of AD cases[55]. CAA has been found to be associated with the degeneration of smooth muscle cells, pericytes and endothelial cells, which moreover contributes to BBB disruption[64].

A study investigating the effects of CAA on penetrating arteriole integrity sampled post-mortem tissue of CAA patients and found a reduction in the volume of vascular smooth muscle[65]. Moreover, arteriolar walls with CAA were found to be 400% stiffer than those without CAA[65]. They noted a strong association with loss of vascular smooth muscle cells/vascular degeneration with lysyl oxidase (LOX), an enzyme responsible for extracellular matrix remodeling/crosslinking[65]. They hypothesize that increased vascular stiffness is likely a result of replacement of vascular smooth muscle cells by Aβ, cross-linking of extracellular matrix by LOX and potentially fibrosis[65].

The cerebrovascular pathological changes associated with AD may account for the increased prevalence of MIs in AD patients. Primarily, it has been shown that in AD patients,

areas of hypoperfusion, such as the cortical watershed region, are more susceptible to the development of MIs, with AD patients exhibiting more than 10-fold greater incidence of microinfarcts in this region[61]. As well, it has been found that microinfarcts are commonly co-localized with amyloid β vessel depositions in humans[9]. Additionally, the severity of CAA appears to be a predictor of cortical microinfarcts[35].

*1.7 3xTg Alzheimer's mouse model*

Alzheimer's disease is the one of the most common neurodegenerative diseases worldwide and thus, time and resources have been dedicated to developing animal models that replicate the complex and progressive nature of the disease. Unfortunately, animal models have not been able to fully recapitulate the heterogeneity of the disease. 3xTg is a commonly used transgenic model that presents with both amyloid and tau pathology as a result of three gene mutations: APP Swedish, MAPT P301L, and PSEN1 M146V, which are associated with familial Alzheimer's disease[68].

3xTg mice develop plaque and tangle neuropathology[68]. This model is progressive as amyloid β deposits are present as early as 6 months and continue to accumulate up to 12 months[68]. Tau pathology is observed at 12 months, typically within the hippocampus[68]. Notably, different papers report different timelines for when these neuropathological features arise, with the most recent study from the LaFerla group characterizing this model[69]. They found 3xTg mice only develop plaques (stained with Thioflavin S) sparsely in females at 12 months and in most females at 18 months (only in the subiculum). Aβ40 and Aβ42 were quantified in detergent soluble (recently produced) and insoluble (within plaques) micro-dissected hippocampus and cortical tissue[69]. Soluble Aβ40 and Aβ42 was present significantly at 18 months in the hippocampus and cortex[69]. Insoluble Aβ40 and Aβ42 increased significantly in the hippocampus and cortex between 4, 12 and 18 months[69]. Tau pathology (phosphorylated tau, as measured by AT8 and pTau217) arose at 12 months and significantly increases only at 18 months[69]. Neurofibrillary tangles, aggregates of phosphorylated tau, were present only at 18 months in the hippocampus[69]. Notably, these pathological features are present significantly in female mice compared to the male mice[69].

### *1.7.1 Vascular changes in 3xTg mice*

Several vascular pathological changes have been observed in 3xTg-AD mice. Specifically, arteriole diameter exhibited a sigmoidal decrease at a rate faster than wildtype mice, in addition to a more rapid decline in arteriolar flow[70]. Moreover, the density of penetrating vessels decreased significantly in 3xTg mice[70]. This is especially relevant as microinfarcts commonly form as a result of penetrating arteriole occlusion due to the bottleneck in perfusion. In 11-month 3xTg mice, cerebrovascular volume is diminished brain wide, and more significantly in the hippocampus, compared to wildtype counterparts[71]. This observation correlates to an increase in thickening of cortical vascular basement membrane, as evident by increased presence of collagen[71]. The 3xTg model also exhibits CAA, an increased perivascular space, and a decrease in pericytes that was found to be associated with cerebral amyloid deposits at 13 months of age[72].

One study investigating whole brain angioarchitecture found an initial increase in vessel segments between 6 and 12 months and a decrease after 24 months in 3xTg mice compared to wildtype mice[73]. Vessel surface area, which plays an important role in solute exchange, significantly decreased at 24 months in 3xTg mice, along with a decrease in the number of vessel connections[73]. Overall complexity of vascular network decreased with age[73]. Here they noted that these differences in cerebrovascular networks between 3xTg and wildtype mice were primarily driven by the microvasculature[73].

### *1.7.2 AD mice and cerebral microinfarcts*

Since microinfarcts and Alzheimer's disease are often co-morbid, it can be difficult to determine which pathology arose first. It can be argued that AD pathology, such as hypoperfusion or CAA, triggers the onset of microinfarcts. Alternatively, it may be suggested that microinfarcts, although likely not triggering the onset of AD, could exacerbate disease pathology. Several papers have investigated these concepts.

Okamoto et al. studied human brain tissue and found CAA to be a multivariate predictor of cortical microinfarcts[35]. To investigate this relationship further, they found that in a mouse mode of CAA (Tg-SwDI), hypoperfusion induced by bilateral carotid stenosis accelerated the deposition of leptomeningeal amyloid β with several mice developing cortical microinfarcts. In CAA mice without hypoperfusion, amyloid β deposits were limited with no signs of

microinfarcts[35]. Similarly, Salvadores et al. used the same CAA model with induced hypoperfusion and were able to detect soluble Aβ at 1 month in the parenchyma and significant levels of insoluble Aβ in the parenchyma and vasculature at 3 months[74]. Moreover, they found that soluble parenchymal Aβ was associated with NOX2 (NADPH oxidase). It is likely that in response to hypoperfusion, the increased production/deposition of Aβ may trigger oxidative stress promoting cerebrovascular disruption and ultimately the development of MIs. Together, these papers suggest hypoperfusion, typically seen in AD, in conjunction with CAA can trigger the onset of MIs.

Backsai et al. investigated the development of amyloid β pathology *in vivo* following the occlusion of microvessels (20-50um in diameter) using a photothrombotic stroke model in 6 month APPswe/PS1dE9 mice[77]. After 7 days, amyloid β plaques developed within the volume of the microinfarct, yet at 14 days, the number of new plaques in the stroke volume compared to adjacent tissue was not significantly different[77]. This suggests that local ischemia results in a transient increase in amyloid β pathology at the site of injury, which they also observed in an MCAO (middle cerebral artery occlusion) model of stroke. Additionally, it was found that CAA progression was nearly 2-fold faster in occluded vessels than non-targeted CAA vessels of the same mouse[77].

Immunohistochemistry was performed to further investigate whether this effect was a result of increased amyloid β production or a decrease in amyloid β clearance. Levels of BACE (β-site amyloid precursor protein cleaving enzyme) and presenlin-1, which play a role in β-amyloid production, where unaffected, as were neprilysin or insulin degrading enzyme, which contribute to amyloid β degradation[77]. Thus, it can be hypothesized that clearance pathways for amyloid β along interstitial fluid drainage routes are disrupted resulting in increased amyloid β at sites of injury[77].

Exploring this, studies have investigated the effects of MIs on the glymphatic system, which plays a key role in waste clearance by removing metabolic waste and neurotoxins. Importantly, it aids in the clearance of amyloid β. Venkat et al. induced microinfarcts via injection of cholesterol crystals in the common carotid of rats and found a decreased expression of AQP-4 surrounding blood vessels that persisted till 6 weeks post-microinfarct induction and correlated with cognitive loss[75]. Moreover, using ex-vivo fluorescent imaging of coronal brain

sections, they found an impairment in cerebrospinal fluid penetration into the parenchyma via the paravascular pathways and pial surfaces[75]. Further, Wang et al. observed similar results in mice following injection of cholesterol crystals[76]. They found global suppression of glymphatic function that resolved 2 weeks post-microinfarct induction. Moreover, the CSF tracers were found to accumulate within tissue associated with microinfarcts. Notably, these observations were exacerbated in aged mice (12 months), compared to young counterparts (2-3 months). They concluded that glymphatic function is focally disrupted in association with microinfarcts and that the aging brain is more vulnerable to this effect[76]. Together, it is possible that microinfarcts trigger glymphatic drainage dysfunction, which ultimately facilitates amyloid β build up.

ElAli et al. also investigated the effect of microinfarcts on Alzheimer's disease pathology on a longer timescale, taking into account sex differences[78]. Sporadic microinfarcts were induced in APP/PS1 mice through the injection of 20um fluorescent microspheres into the carotid artery. It was found that microinfarcts reduced amyloid β deposits, while soluble levels of amyloid β were unaffected[78]. Moreover, male mice exhibited rapid and prolonged cognitive deficits, while females exhibited mild and transient cognitive deficits, as determined by the novel object recognition test and open field test[78]. Additionally, male mice displayed acute and chronic hypoperfusion, while female mice only experienced hypoperfusion in the acute stage[78]. Interestingly, female mice had a more robust microglial response and recruitment of peripheral monocytes to the site of injury and amyloid β plaques, which could be a possible explanation for the reduced Aβ deposition in female mice[78]. Lastly, CAA was found to decrease in female AD mice post-microinfarct induction[78]. Here they hypothesized that a reduction in amyloid β deposition, primarily in females, is a result of immune cell recruitment following microvessel occlusion which aids in amyloid β clearance.

*1.8 Experimental rationale*

It is evident that microinfarcts are abundant in the human population, particularly in the aging population and those with diagnosed dementia[3]. However, the relationship between aging/AD and microinfarcts is still largely unknown.

The timeline of angiophagy in young mice has been previously established by Lam et al. and van der Wijk et al. However, these previous studies fall short in thoroughly quantifying angiophagy with appropriate sample sizes. van der Wijk's 2019 study quantified 40-42

microspheres total (from 4 rats) at each time point and the 2020 study quantified only 195 and 53 microspheres for each of the different size microspheres (15 and 20um respectively)[38,39]. Interestingly, these two papers published by the same group one year apart, claim significantly different rates of angiophagy when comparing between the same size microspheres, with extravasation rates of 76% compared to 33% at day 7. Between the previously published studies investigating angiophagy, there appears to be inconsistent findings and an inability to replicate results.

Additionally, angiophagy in aging has limited data presented by Lam et al. and angiophagy in Alzheimer's disease has yet to be explored. Pathological cerebrovascular changes are observed in both aged and Alzheimer's disease and may lead to a disruption of the process of angiophagy, which could be a possible explanation as to why microinfarcts are more commonly present in the aging population and Alzheimer's disease patients.

## *2 Methods*

### *2.1 Animals and experimental timeline*

Male and female Tmem119-2A-EGFP mice were used for the young wildtype cohort (The Jackson Laboratory, strain #031823). These knock-in mice allow for visualization of central nervous system microglia via fluorescently labelled transmembrane protein 119 (Tmem-119) with EGFP[68]. Due to weak fluorescence signal in our histological sections, microglial fluorescence was not quantified in these experiments. The mice were between 2 and 6 months of age.

In addition to Tmem-119 mice, male and female Thy1-ChR2-YFP mice were also used for the aged wildtype cohort (The Jackson Laboratory, strain #007612). This mouse line expresses the light-gated cation channel ChR2 in a subpopulation of cortical neurons, which may be utilized in subsequent experiments[69]. Importantly, both mouse lines are C57BL6 strains with no known phenotypes. The mice are between 9 and 20 months of age.

Male and female 3xTg-AD mice were used for our Alzheimer's model (The Jackson Laboratory, strain #034830), with the non-transgenic, strain-matched controls (The Jackson Laboratory, strain #101045). The young cohort was 2-5 months old, while the aged cohort is 14-16 months old, age-matched between 3xTg and NTG mice.

Following surgery (D0), mice were sacrificed at 3 experimental timepoints: day 3, day 7, and day 14.

*2.2 Surgical preparation and protocol*

A fluorescent microsphere model of microinfarction was used, first described by Silasi et al.[23]. A solution of approximately 4000 microspheres/100$\mu$L injection was prepared prior to surgery using stock solution of fluorescent microspheres (FluoroSpheres polystyrene, Polysciences, Cat# 19096-2; 20um particles, 2.5% aqueous suspension 5.68 x 10^6 particles/mL). A 5$\mu$L sample was taken from the final prepared microsphere solution and imaged under Ziess Axio Imager M2. After thresholding the acquired image of the solution sample in ImageJ, the Particle Analyze function was used to count the number of microspheres present in the 5$\mu$L sample. The solution was adjusted accordingly to a final concentration of approximately 4000 microspheres/100$\mu$L. During surgery, prior to injection, the microsphere solution was vortexed for approximately 30 seconds to ensure the solution was mixed and the microspheres were separated.

In preparation for the surgery, mice were placed in an induction chamber and anesthetized via inhalation of isoflurane (3.5%) for 3 minutes with oxygen set to flow at 1L/min. Following initial anesthetization (confirming with toe pinch), mice were placed in the prone position on a heating pad set to 37ºC to maintain homeostatic temperature with 2% isofluorane-1L/min oxygen. Meloxicam (0.5mg/mL, 0.1mL/10g per animal) was injected subcutaneously and Optixcare eye lubricant was applied to the eyes to avoid drying. In the supine position, fur on the upper chest and neck was shaved with an electric razor followed by 70% isopropyl alcohol and chlorohexidine gluconate swab for disinfection.

A surgical incision at the neck (approximately 1.5cm) was created to gain access to the common carotid artery (CCA). Under a dissecting microscope, the internal carotid artery was isolated, while a microvascular clamp was used to temporarily block the external carotid artery. A 31G needle was used to inject 100$\mu$L of the microsphere solution (4000 microspheres/100$\mu$L) into the common carotid artery at a steady rate (over approximately 30 seconds). The microspheres stochastically distribute throughout the hemisphere and become lodged in penetrating arterioles. The clamp was removed from the external carotid artery and surgifoam was applied to control bleeding. The incision was sutured, followed by application of

bupivacaine (2% transdermal, 0.1mL per animal) and mice recovered in a 30ºC incubator prior to returning to their home cage.

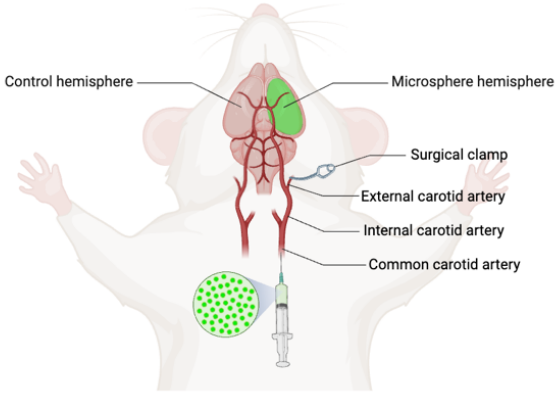


**Figure 1. Rodent model of microinfarction**. ~4000 fluorescent microspheres are injected into the left common carotid artery of an anesthetized mouse. The microspheres stochastically distribute and become lodged in the microvasculature of the brain forming microinfarcts. Method derived by Silasi et al. (2015).

*2.2 Euthanization and vascular labelling*

Mice were anesthetized with an intraperitoneal injection of sodium pentobarbital (65mg/mL, 10mL/kg). After confirming lack of responsiveness to a toe pinch, an incision was made to open the thoracic cavity. For visualization of the cerebral vasculature, 100$\mu$L of Evans Blue (EB) (Sigma E2129, MW: 960.8g/mol, 2% solution in saline) was injected into the left ventricle of the heart with a 31G needle. The EB dye was allowed to circulate for a minimum of 5 minutes prior to extracting the brain. Brains were not perfused, so as to retain both microspheres and vascular labeling. Instead, they were post-fixed in 4% paraformaldehyde, at minimum for 24 hours, and stored at 4 ºC until further processing.

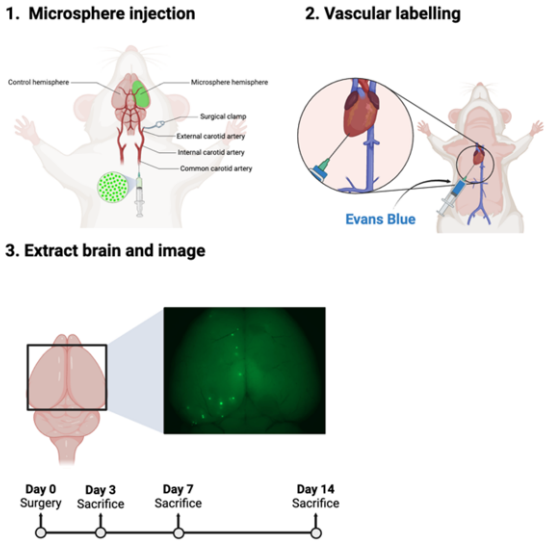


**Figure 2. Experimental design.** Mice undergo microinfarct surgery and are sacrificed on day 3, day 7 or day 14. Evans Blue is injected intracardially and allowed to circulate prior to sacrifice. The brain is then extracted and sectioned at 100$\mu$m. Coronal sections are imaged at 2.5x on a fluorescence microscopy.

*2.3 Histological processing*

Brains were sectioned at 100$\mu$m thickness on a vibratome and sections were placed on 1% gelatin-coated slides. Slides were coverslipped with Fluoromount-G prior prior to imaging on the Ziess Axio Imager M2. For angiophagy quantification, individual microspheres (GFP; 510nm emission) and vessels (Evans Blue; 610nm emission) were imaged at 20x magnification. For brain-wide quantification and localization of microspheres, sections were tile-scanned at 2.5x (GFP; 510nm emission) and stitched in Zen software.

*2.4 Microsphere Localization and Quantification*

The previously defined semi-automated QUINT workflow was used for quantification and spatial analysis of microspheres on a brain-wide scale[70]. The image analysis pipeline consists of three open source software packages: Ilastik, QuickNII and Nutil. Raw image files acquired

from the Ziess Axio Imager M2 at 10x were pre-processed with IrfanView (serial order and batch rename), Nutil (resize), and ImageJ (rotate).

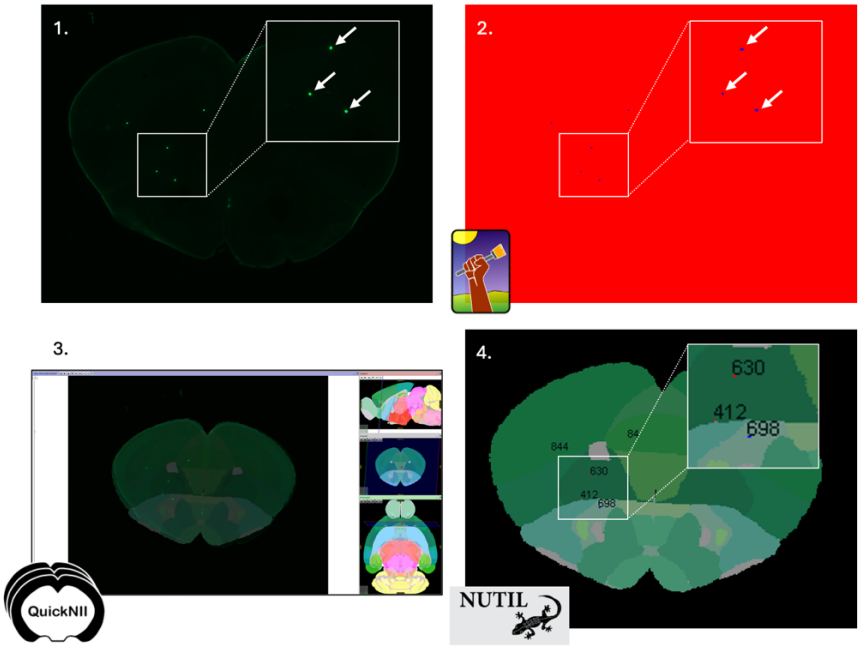


**Figure 3. QUINT Image Analysis Workflow.** 100$\mu$m coronal sections are imaged at 2.5x with fluorescence microscopy**(1)**. Images are pre-processed and uploaded to Ilastik to generate segmentation files **(2)**. Section images are uploaded to QuickNII for alignment with the Allen Mouse Brain Atlas **(3)**. Nutil combines the Ilastik and QuickNII outputs to generate reports on microsphere quantification and distribution **(4)**.

The Pixel Classification tool in Ilastik is used to generate segmentation files to differentiate the microspheres from the background. 10% of total acquired sections (approximately 7 images) were used to train the Pixel Classifiers in Ilastik. Annotations were applied to mark the microspheres against the background. Additional annotations were added to improve accuracy of predicted pixel classification, which is made based on pixel size, intensity and colour. The images were manually assessed and annotated until it was found the microspheres were correctly identified across all training images. The remaining serial sections were imported and the trained classifier generated segmentation maps for the whole series using the batch application feature. Batch processing in ImageJ was used to visualize segmentation files in colour with the glasbey lookup table.

In QuickNII (RRID: SCR_016854), the acquired serial sections of the experimental brain are superimposed with the atlas (Allen Mouse Brain 2017) to allow for manual alignment, taking into account the size, position, orientation and sectioning angle. Predetermined landmarks are typically aligned first (development of corpus callosum, anterior commissures, and anterior hippocampus), followed by the remaining sections. Exported from QuickNII are the manually-adjusted serial alignments of the experimental and reference atlas sections with an XML file describing a set of vectors regarding image position in relation to the atlas.

Using the quantifier feature in Nutil, microsphere quantification and localization can be obtained. The Ilastik segmentation files, QuickNII alignment files, and the QuickNII XML file are imported into Nutil. Nutil generates a list of objects (microspheres) and assigns a label ID that corresponds to the reference atlas and the object's spatial coordinates. Relevant for our use, the final output details the number of microspheres in each brain region (cortex, fibretracts, hippocampus, olfactory, midbrain/hindbrain/medulla, thalamus, and ventricular system) and the size of the region. Microsphere distribution was normalized to region area by dividing the number of microspheres in a given region by the size of the region as determined by Nutil.

*2.5 Quantification of Angiophagy*

The timeline of angiophagy was quantified based on the location of the bead in relation to the nearest visible vessel (labelled with Evans Blue) and was categorized into one of three classifications: obstructed, going out, or externalized. Given that there are upwards of 1500 microspheres per brain, up to 20 microspheres (minimum 5 microspheres) were quantified per brain region (cortex, striatum, hippocampus, thalamus and hypothalamus), with a minimum of 10 and maximum of 100 microspheres quantified brain wide at random.

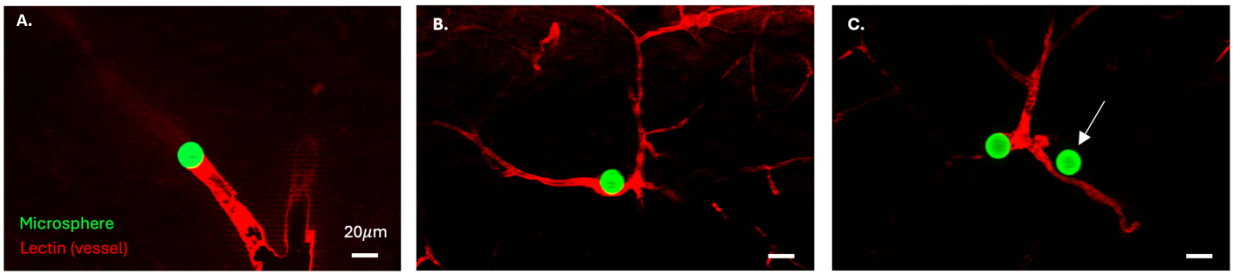


**Figure 4. Classification of angiophagy timeline.** 20$\mu$m fluorescent microspheres targeted to the left hemisphere with vessel labeling via tail vein injection of lectin prior to sacrifice. Images of coronal sections captured with fluorescence microscopy at 20x. Angiophagy was quantified by classifying images into one of three categories based on microsphere (green) location in relation to the vessel (red): obstructed **(A)**, going out **(B)** and extravasated **(C)**.

*2.6 Statistical Analyses*

All values were expressed as mean ± standard error of mean (SEM). All statistical analyses were performed in GraphPad Prism 10 (San Diego, CA, USA). One-way analysis of variance (ANOVA) followed by Tukey's multiple comparison was used to analyze microsphere distribution across cohorts. Two-way ANOVA with Tukey's multiple comparison was used to analyze microsphere localization across regions/cohorts and quantification of angiophagy. All p-values $< 0.05$ were considered significant. To analyze the correlation plots, Pearson's bivariate correlation was used.

*3 Results*

*3.1 Microspheres primarily localize to the neocortex across all experimental cohorts*

Using the semi-automated QUINT image analysis pipeline, we determined the total number of microspheres per brain sample. Across the experimental groups, the young non-diseased, aged non-diseased and aged 3xTg cohorts had the fewest number of microspheres brain wide with a mean of 524.2±115.3, 490.5±68.62 and 531.0±185.7 microspheres, respectively (Figure 5). The young NTG, young 3xTg and aged NTG cohorts had the greatest number of microspheres brain wide with a mean of 890.7±90.75, 835.7±95.67, and 779.0±172.4 microspheres, respectively (Figure 5). All animals with less than 50 microspheres in the brain were considered unsuccessful injections and excluded from analysis (n=17).

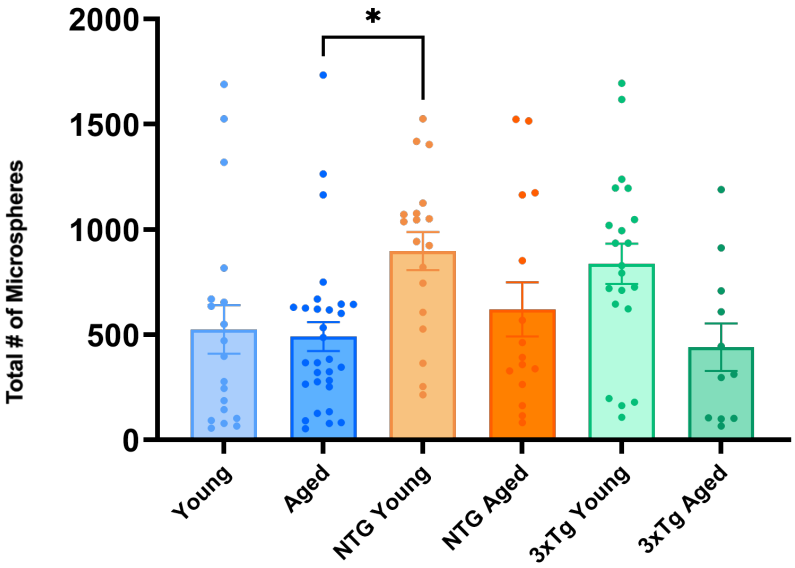


**Figure 5. Microsphere quantification across experimental cohorts.** Using a semi-automated image analysis pipeline, microsphere load was quantified in each experimental cohort. Animals with less than 50 microspheres in the brain were excluded. Data expressed as mean ± SEM. One-way ANOVA with Tukey's multiple comparison. *$p<0.05$.

We were also able to determine the regional distribution of microspheres and found that the greatest number of microspheres localized to the neocortex across all experimental cohorts (Figures 6). The region with the second greatest percent of microspheres was determined to be the hippocampus for the young non-diseased and aged NTG cohorts, the thalamus for the aged non-diseased and young NTG cohort and the striatum/pallidum for the young 3xTg and aged 3xTg cohorts (Figures 6). When comparing the percent of microspheres within each brain region, there was no significant difference between the experimental cohorts (Figure 6).

When we normalized the number of microspheres by the area (pixels) of each brain region, as determined through the image analysis pipeline, we found that the thalamus had the most microspheres per area of structure across all cohorts (Figure 7). The value varied slightly between experimental cohorts, with significantly more microspheres per region area in the thalamus of the young NTG cohort compared to the young non-diseased, aged NTG and aged 3xTg cohorts and in the hypothalamus of the young NTG group compared to the young non-diseased and the aged 3xTg cohorts (Figure 7).

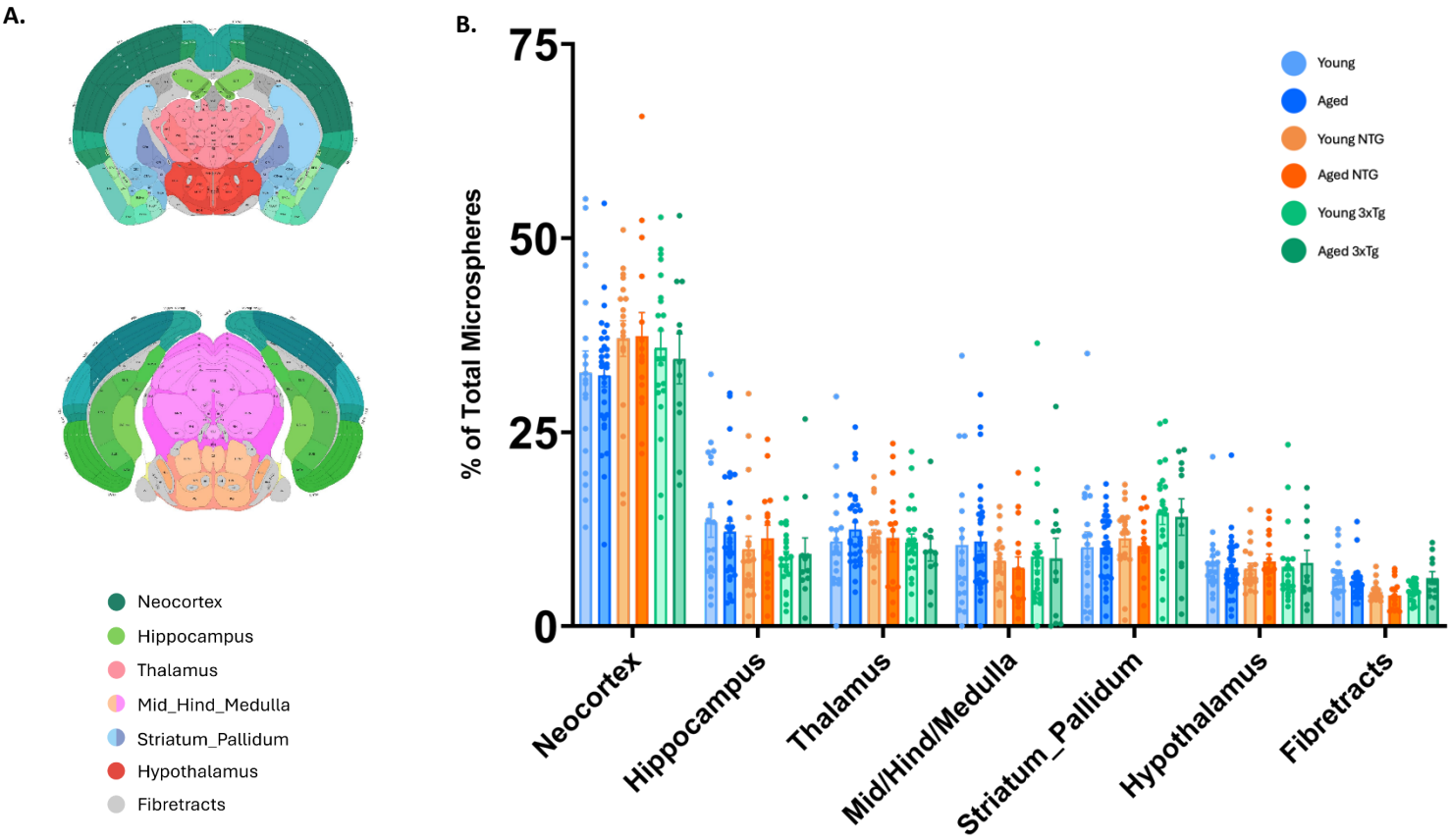


**Figure 6. Microsphere localization for all experimental cohorts.** Using a semi-automated image analysis pipeline, microsphere localization was determined in young non-diseased, aged non-diseased, young NTG, aged NTG, young 3xTg, and aged 3xTg mice. **(A)** Allen Mouse Brain Atlas for the region legend. **(B)** Regional microsphere localization. Regions not shown: olfactory, ventricular system, cerebellum. Data expressed as mean ± SEM. Two-way ANOVA with Tukey's multiple comparison.

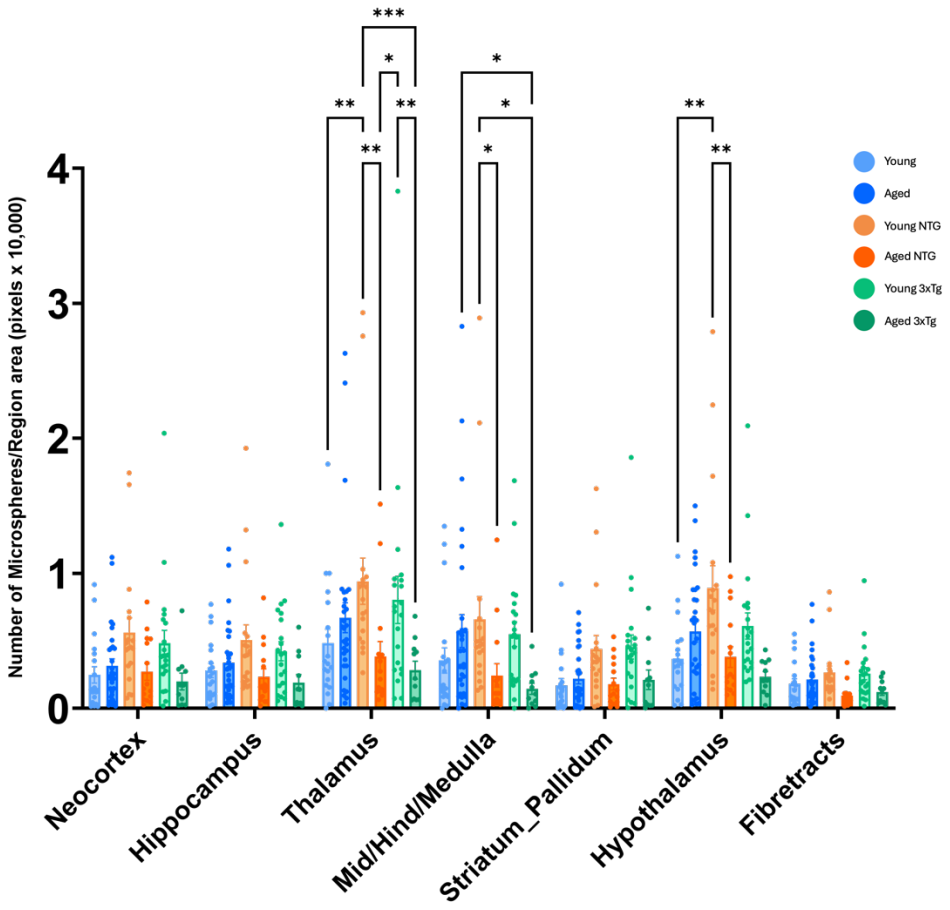


**Figure 7. Normalized microsphere localization for all experimental cohorts.** Using a semi-automated image analysis pipeline, microsphere localization was determined in young non-diseased, aged non-diseased, young NTG, aged NTG, young 3xTg, and aged 3xTg mice. Regional distribution of microspheres was normalized to size of brain region as determined by Nutil. Regions not shown: olfactory, ventricular system, cerebellum. Data expressed as mean ± SEM. Two-way ANOVA with Tukey's multiple comparison. **p<0.01, *p<0.05.

*3.2 Angiophagy is delayed in aged, non-diseased mice*

To determine a time course of angiophagy, we quantified the process over the course of 3 timepoints: day 3, 7, and 14. Using fluorescent microscopy, the microspheres were categorized into one of three groups depending on its location in relation to the vessel: obstructing the vessel, in the process of going out of the vessel, and extravasated outside of the vessel.

In the young cohort, the percent of microspheres obstructing the vessels decreased from 83.9146±2.5868% at day 3 to 39.12±5.3162% at day 14, while the percent of extravasated microspheres increased from 11.5715±2.6715% at day 3 to 43.8528±2.95315% at day 14 (Figure 8). The rate of angiophagy did not differ significantly across brain regions, except in the obstructing stage whereby the white matter had a greater percent of obstructing microspheres compared to the thalamus at day 7 (Figure 9).

In the aged cohort, a comparable trend was observed whereby the percent of microspheres obstructing the vessels also decreased across time, from 94.6754±1.0887% at day 3 to 80.5360±2.8542% at day 14, while the percent of extravasated microspheres increased from 3.1315±0.8827% at day 3 to 10.6434±2.3788% at day 14 (Figure 8). The rate of angiophagy did not differ significantly across brain regions in the aged cohort except in the going out stage whereby white matter had a greater percent of microspheres going out compared to the striatum at day 14 (Figure 10).

In comparing young and aged non-diseased mice, it was determined the percent of microspheres obstructing a vessel is significantly greater and the percent of extravasated microspheres is significantly less in the aged mice compared to the young mice across all three time points (day 3, 7 and 14) (Figure 8).

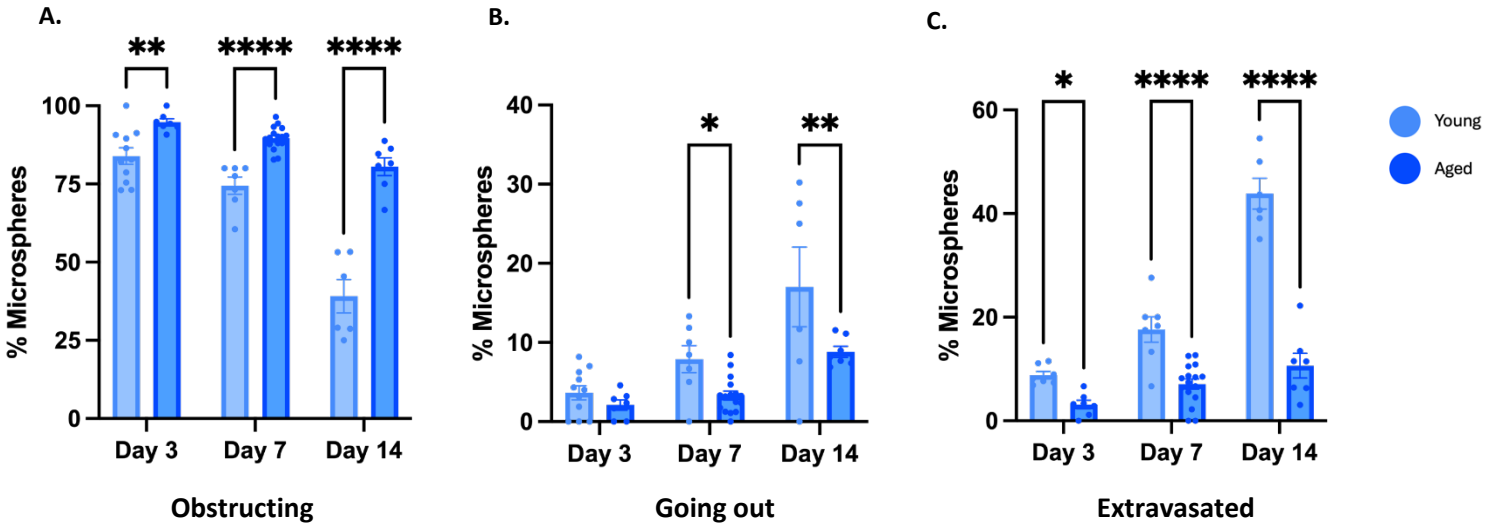


**Figure 8. Quantification of angiophagy in young and aged non-diseased mice.** Microspheres were quantified as **(A)** obstructing the vessel, **(B)** going out of the vessel, and **(C)** extravasated from the vessel at day 3, 7, and 14. Data expressed as mean ± SEM. Two-way ANOVA with Tukey's multiple comparison. ****p<0.0001, **p<0.01, *p<0.05.

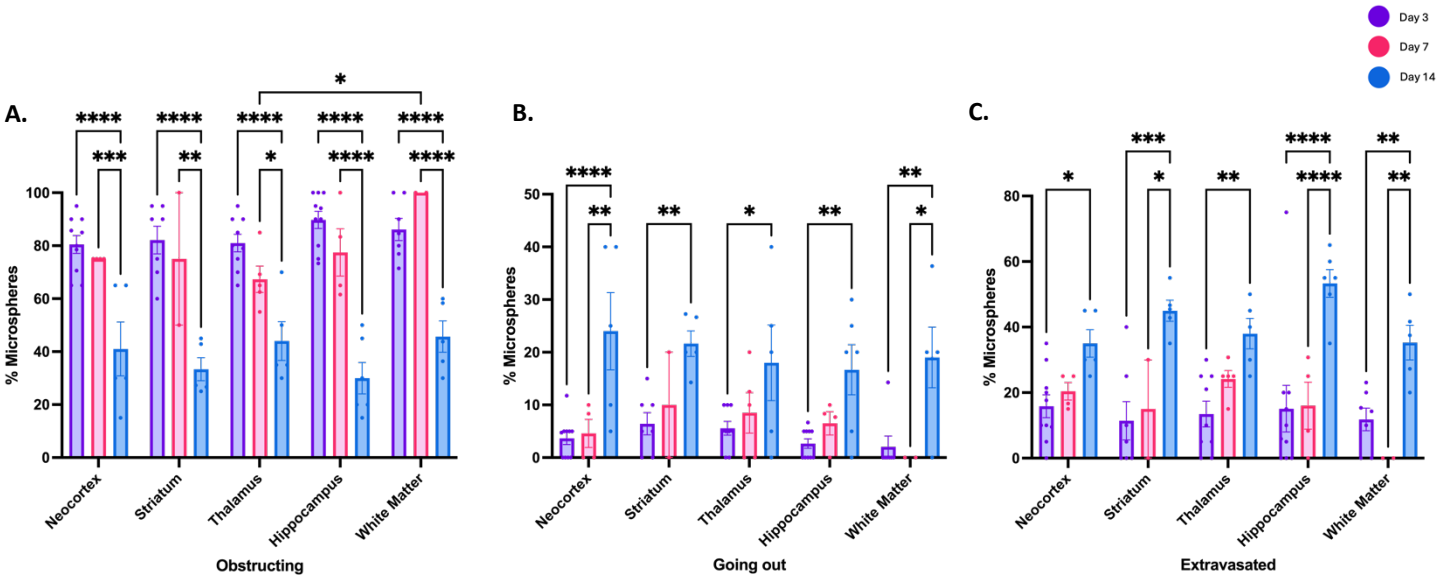


**Figure 9. Quantification of angiophagy per brain region in young non-diseased mice.** Microspheres were quantified as **(A)** obstructing the vessel, **(B)** going out of the vessel, and **(C)** extravasated from the vessel in each of five brain regions: neocortex, striatum, thalamus, hippocampus, and white matter at day 3, 7, and 14. Data expressed as mean ± SEM. Two-way ANOVA with Tukey's multiple comparison. ****p<0.0001, ***p<0.001, **p<0.01, *p<0.05.

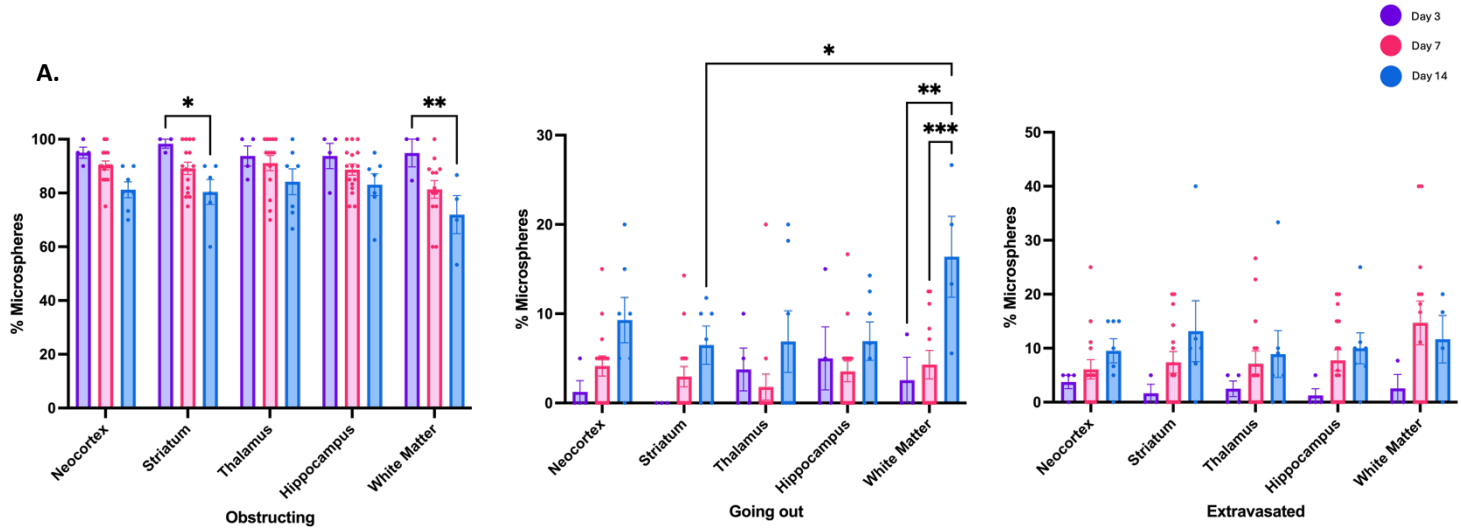


**Figure 10. Quantification of angiophagy per brain region in aged non-diseased mice.** Microspheres were quantified as **(A)** obstructing the vessel, **(B)** going out of the vessel, and **(C)** extravasated from the vessel in each of five brain regions: neocortex, striatum, thalamus, hippocampus, and white matter at day 3, 7, and 14. Data expressed as mean ± SEM. Two-way ANOVA with Tukey's multiple comparison. ***p<0.001, **p<0.01, *p<0.05.

*3.3 Increased angiophagy efficiency in Alzheimer's disease mice compared to non-transgenic controls*

In young NTG mice, the percent of microspheres obstructing the vessels decreased from 97.5204±0.7024% at day 3 to 37.7059±4.024% at day 14 (Figure 11). The percent of extravasated microspheres increased across all timepoints, from 1.3037±0.3903% at day 3 to 43.4472±3.1614% at day 14 (Figure 11).

A comparable trend holds true in the young 3xTG mice whereby the percent of microspheres obstructing vessels also decreased overtime from 96.4933±1.0836% at day 3 to 23.6508±2.7848% at day 14, while the percent of extravasated microspheres increased from 1.8985±0.4816% at day 3 to 47.0499±2.5693% at day 14 (Figure 11).

In the aged NTG mice, the percent of microspheres obstructing the vessels decreased from 82.7067±3.6126% at day 7 to 58.3374±3.9471% at day 14 (Figure 11). The percent of extravasated microspheres increased from 13.6290±2.610% at day 7 to 30.3723±4.7717% at day 14 (Figure 11).

In the aged 3xTg mice, a comparable trend was observed whereby the percent of microspheres obstructing the vessels decreased from 87.5013±2.3555% at day 7 to 36.5088±5.8293% at day 14 (Figure 11). The percent of extravasated microspheres increased from 7.6892±0.8216% at day 7 to 38.0953±4.7717% at day 14 (Figure 11).

The rate of angiophagy across regions did not differ significantly for all experimental cohorts (Figure 12-15).

When comparing angiophagy between NTG and 3xTg cohorts at each timepoint, we see that 3xTg mice are generally more efficient at this process of angiophagy. This is particularly evident at day 14 whereby the young and aged 3xTg mice have less microspheres obstructing the vessels, and more microspheres in the process of going out and extravasated compared to the NTG groups. There is a significant difference between the aged NTG and aged 3xTg cohorts at day 7 and day 14, whereby 3xTg mice have a greater percent of microspheres in the process of leaving the vessel compared to NTG mice (Figure 11).

Comparing young vs aged mice in the NTG cohort, a significance difference was observed at the day 7 and 14 timepoint, whereby the aged cohorts have a significantly greater percent of microspheres obstructing the vessel and significantly fewer microspheres going out compared to the young cohort (Figure 11). In the 3xTg cohort, a significant difference in the percent of

microspheres obstructing vessels was present at day 7 and 14, whereby the aged cohort have a significantly greater percent of obstructed vessels than the young 3xTg cohort (Figure 11).

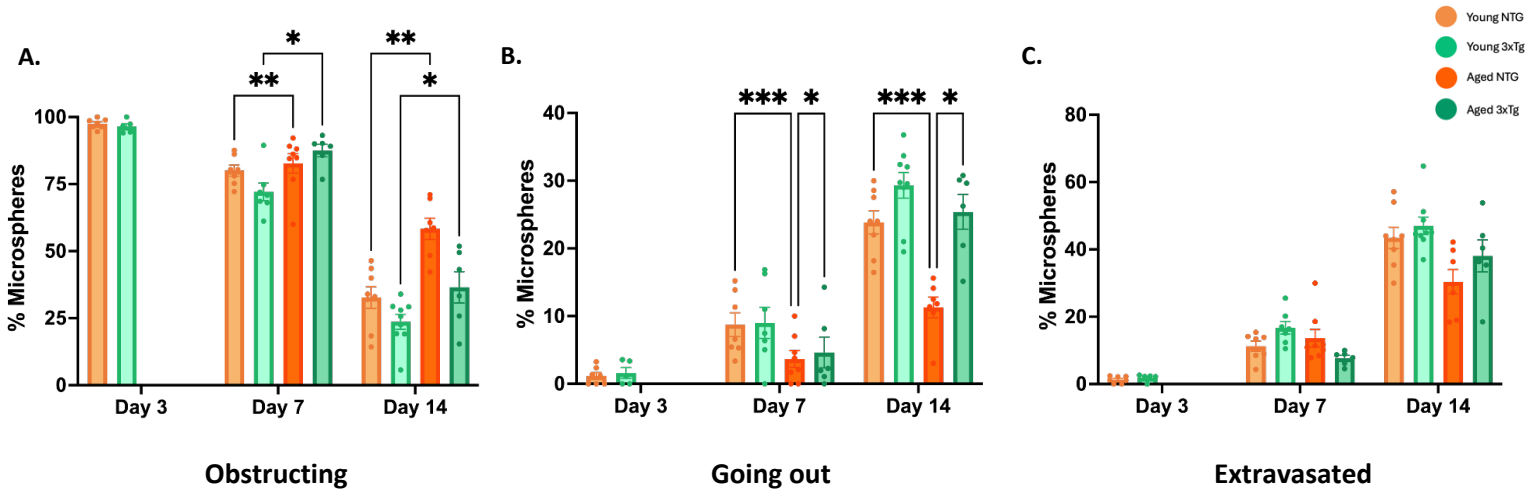


**Figure 11. Quantification of angiophagy in young/aged NTG/3xTg mice.** Microspheres were quantified as **(A)** obstructing the vessel, **(B)** going out of the vessel, and **(C)** extravasated from the vessel at day 3, 7, and 14 in young NTG/3xTg mice and day 7 and 14 in aged NTG/3xTg mice. Data expressed as mean ± SEM. Two-way ANOVA with Tukey's multiple comparison. ***p<0.001, **p<0.01, *p<0.05.

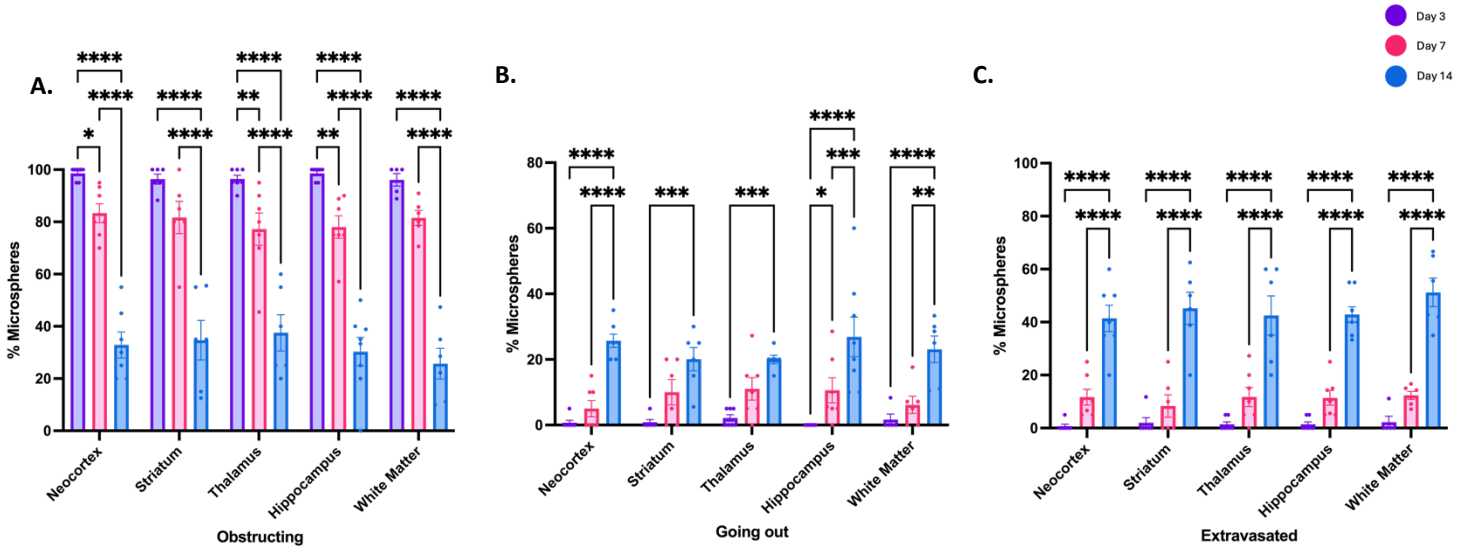


**Figure 12. Quantification of angiophagy per brain region in young NTG mice.** Microspheres were quantified as **(A)** obstructing the vessel, **(B)** going out of the vessel, and **(C)** extravasated from the vessel in each of five brain regions: neocortex, striatum, thalamus, hippocampus, and white matter at day 3, 7, and 14. Data expressed as mean ± SEM. Two-way ANOVA with Tukey's multiple comparison. ****p<0.0001, ***p<0.001, **p<0.01, *p<0.05.

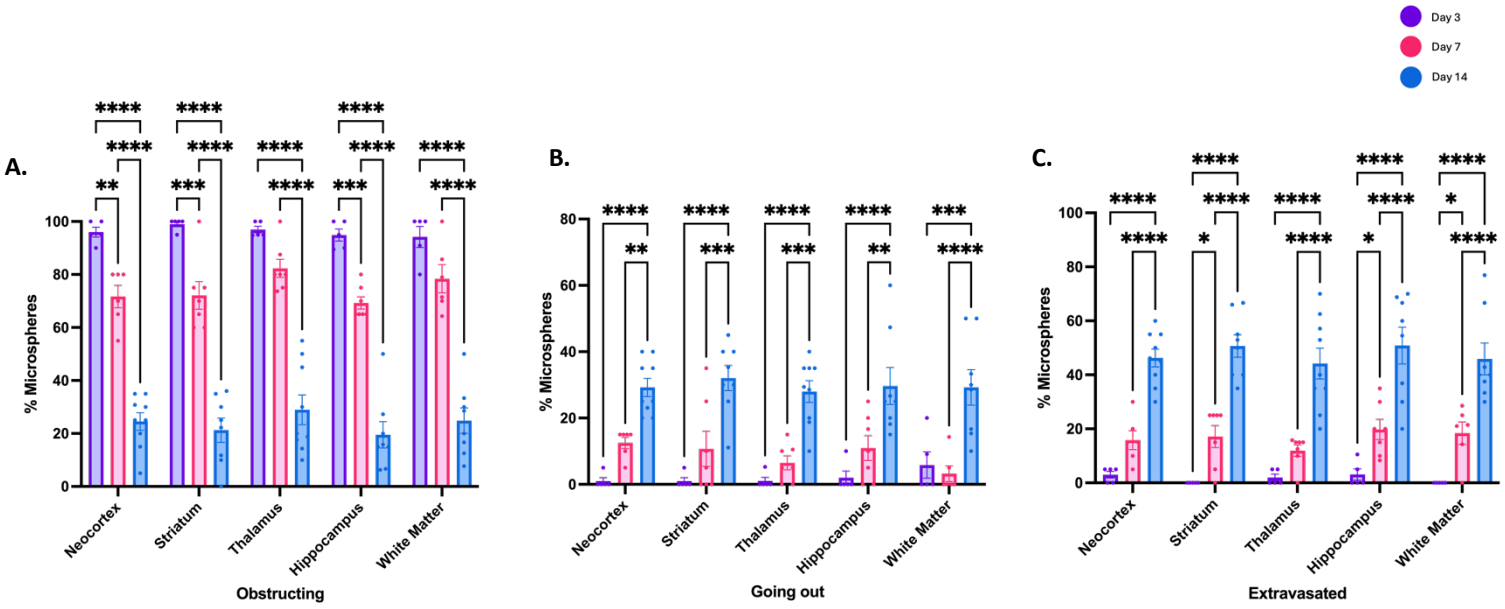


**Figure 13. Quantification of angiophagy per brain region in young 3xTG mice.** Microspheres were quantified as **(A)** obstructing the vessel, **(B)** going out of the vessel, and **(C)** extravasated from the vessel in each of five brain regions: neocortex, striatum, thalamus, hippocampus, and white matter at day 3, 7, and 14. Data expressed as mean ± SEM. Two-way ANOVA with Tukey's multiple comparison. ****p<0.0001, ***p<0.001, **p<0.01, *p<0.05.

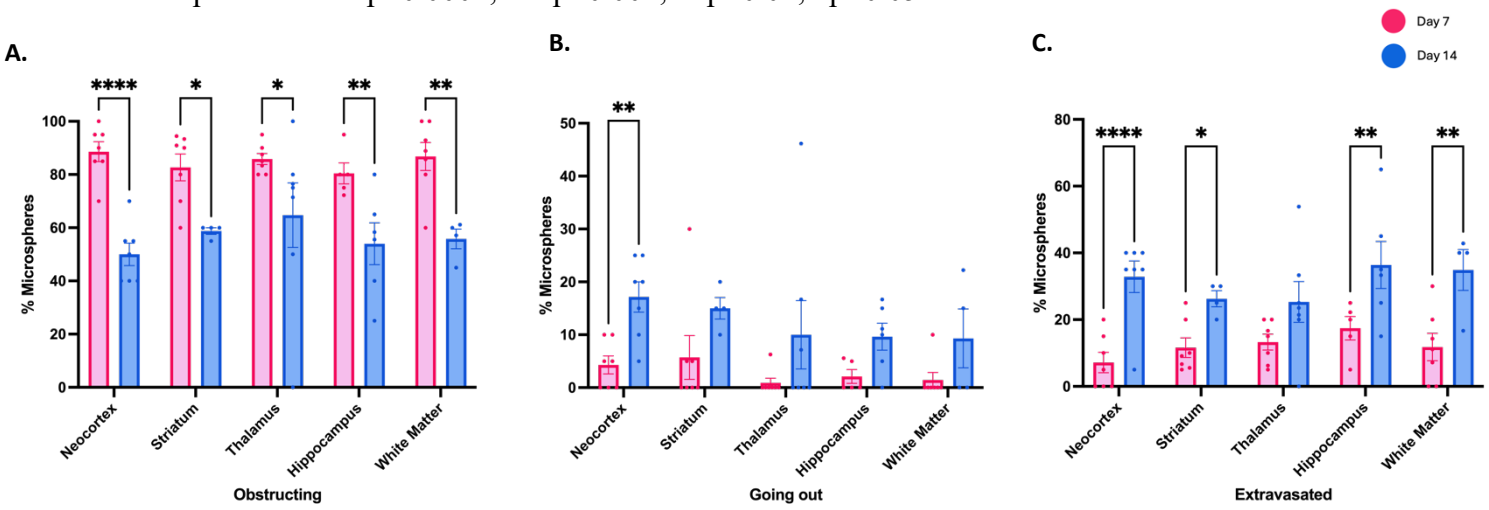


**Figure 14. Quantification of angiophagy per brain region in aged NTG mice.** Microspheres were quantified as **(A)** obstructing the vessel, **(B)** going out of the vessel, and **(C)** extravasated from the vessel in each of five brain regions: neocortex, striatum, thalamus, hippocampus, and white matter at day 3, 7, and 14. Data expressed as mean ± SEM. Two-way ANOVA with Tukey's multiple comparison. ****p<0.0001, **p<0.01, *p<0.05.

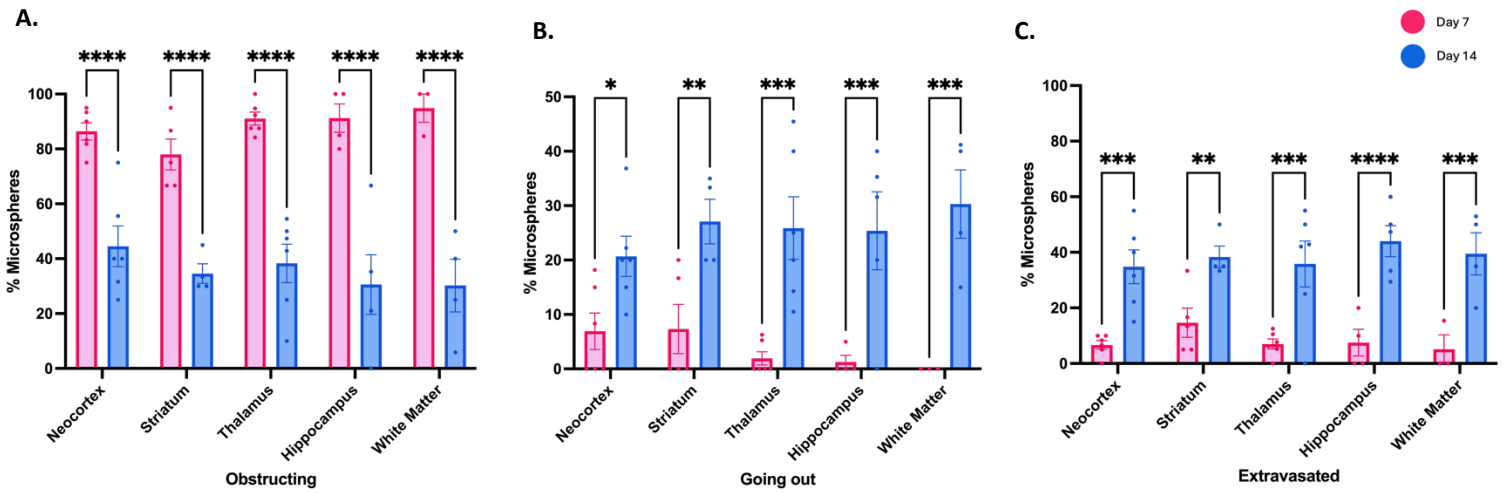


**Figure 15. Quantification of angiophagy per brain region in aged 3xTg mice.** Microspheres were quantified as **(A)** obstructing the vessel, **(B)** going out of the vessel, and **(C)** extravasated from the vessel in each of five brain regions: neocortex, striatum, thalamus, hippocampus, and white matter at day 3, 7, and 14. Data expressed as mean ± SEM. Two-way ANOVA with Tukey's multiple comparison. ****p<0.0001, ***p<0.001, **p<0.01, *p<0.05.

*3.4 Correlations between microsphere load and the occurrence of angiophagy*

Correlation plots were created to investigate a potential relationship between microsphere load and rate of angiophagy. Microsphere load was graphed against extravasated microspheres at each timepoint for the young cohorts (combined) and aged non-diseased cohorts (Figures 16 and 17). Across the young cohorts, day 3 and 14 had a positive correlation, whereby a greater microsphere load correlates to a greater percent of extravasated microspheres, or increased occurrence of angiophagy (Figure 16). In the aged cohort, days 3 and 7 had a positive correlation (Figure 17). The young cohorts at day 7 and the aged non-diseased cohort at day 14 appears to have a general negative correlation, whereby a greater microsphere load correlates to less extravasated microspheres, or a decreased occurrence of angiophagy (Figure 16 and 17). Correlation between microsphere load and percent of extravasated microspheres is only significant in the aged non-diseased mice at day 3 with an r value of 0.8548 (Figure 17).

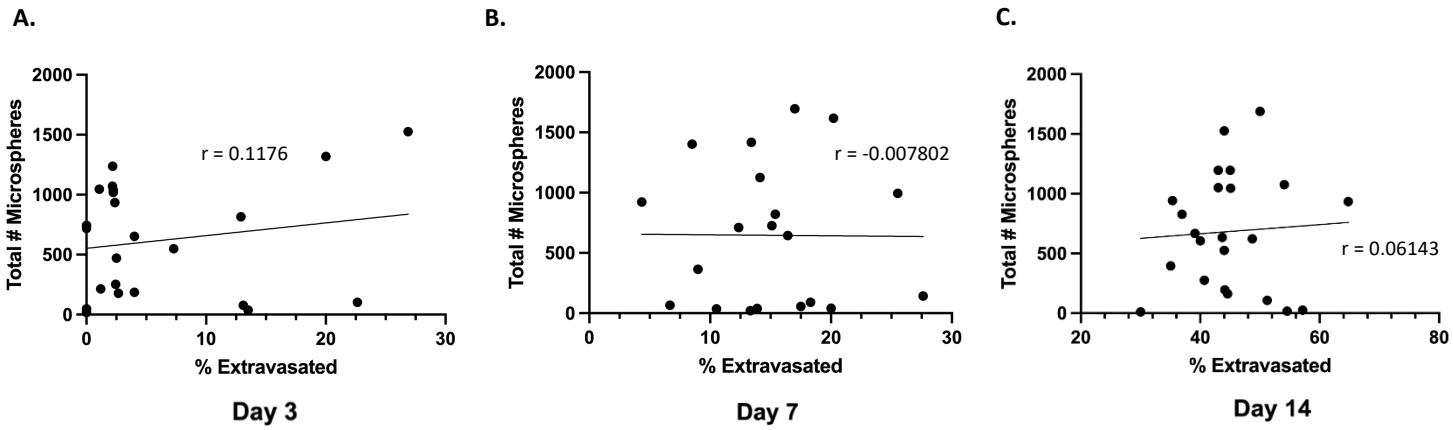


**Figure 16. Correlation between microsphere load and extravasated microspheres (%) in young non-diseased, young NTG and young 3xTg mice.** Correlation between microsphere load and extravasated microspheres at day 3 **(A)**, day 7 **(B)** and day 14 **(C)** in all young mice.

| Day | 3 | 7 | 14 |
|---|---|---|---|
| Pearson r | 0.1176 | -0.007802 | 0.06143 |
| 95% confidence interval | -0.2531 to 0.5496 | -0.4488 to 0.4362 | -0.3599 to 0.4619 |
| R squared | 0.03155 | 6.087e-005 | 0.003774 |
| P value (two-tailed) | 0.4175 | 0.9470 | 0.7807 |
| P value summary | ns | ns | ns |
| Significant? (alpha = 0.05) | No | No | No |
| Number of XY pairs | 23 | 20 | 23 |

**Table 1.** Correlation results for microsphere load and extravasated microspheres (%) in young non-diseased, young NTG and young 3xTg mice combined.

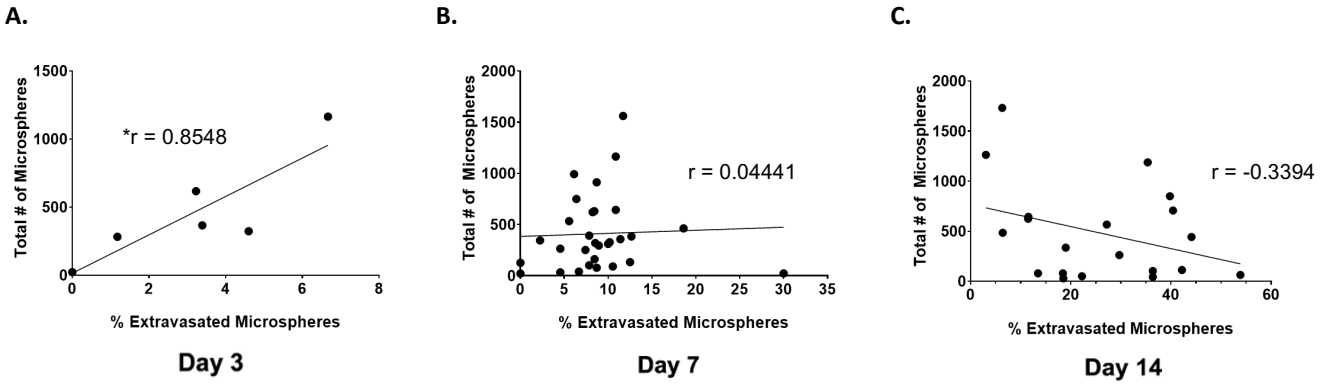


**Figure 17. Correlation between microsphere load and extravasated microspheres (%) in aged non-diseased mice, aged NTG and aged 3xTg mice.** Correlation between microsphere load and extravasated microspheres at day 3 **(A)**, day 7 **(B)** and day 14 **(C)** in all aged mice. * = significant (alpha = 0.05).

| Day | 3 | 7 | 14 |
|---|---|---|---|
| Pearson r | 0.8548 | 0.04441 | -0.3394 |
| 95% confidence interval | 0.1411 to 0.9838 | -0.3210 to 0.3983 | -0.6798 to 0.1213 |
| R squared | 0.7307 | 0.001972 | 0.1152 |
| P value (two-tailed) | 0.0301 | 0.8157 | 0.1432 |
| P value summary | * | NS | NS |
| Significant? (alpha = 0.05) | Yes | No | No |
| Number of XY pairs | 6 | 30 | 20 |

**Table 2.** Correlation results for microsphere load and extravasated microspheres (%) in aged non-diseased, aged NTG and aged 3xTg mice.

*4 Discussion*

Microvessel occlusions are a common cause of microinfarcts[1]. The brain has protective mechanisms in place to clear microemboli including washout via hemodynamic forces and chemical breakdown of clots[49]. Moreover, angiophagy has been found to facilitate reperfusion as a prominent clearance mechanism[50]. In the first report of this process, Lam et al. proposed that 80% of microemboli were cleared from vessels through this process of vascular remodeling 8 days following delivery of microemboli to the brain[50]. Using the injection of fluorescent polystyrene microspheres to model microinfarcts in mice, we investigated this process of angiophagy over the course of 14 days and found that approximately 43% of quantified microspheres had undergone extravasation at this timepoint. This process was found to be

delayed in aged mice, which aligns with current literature. Novel to our study, we observed a general decrease in the percent of microspheres obstructing vessels and an increase in the percent of microspheres going out and extravasated from vessels in young and aged 3xTg mice, primarily at day 14, suggesting an increase in the process of angiophagy in this AD mouse model.

*4.1 Microsphere load comparable across experimental cohorts*

The diffuse emboli model is commonly used to study microinfarcts and emboli clearance mechanisms. Using the semi-automated QUINT analysis pipeline, we were able to quantify and localize all microspheres in the brain[81]. Our findings suggest variability in the number of microspheres between samples, despite using a consistent concentration of microsphere solution across surgeries. Following the injection of microemboli into the carotid artery, it has become evident that not all microspheres reach the brain, potentially as a result of unsuccessful/partial injections or the microspheres ability to circulate out of the brain prior to endpoint.

Some studies have quantified the total number of microspheres present in the brain compared to the number of microspheres injected. Silasi et al. found a mean of 423 microspheres in the brain with 2000 microspheres injected, McDonald et al. found a mean of 303 microspheres with 2000 microspheres injected, and van Der Wijk et al. found a mean of 937 microspheres with 31,125 microsphere injected[23,30,40]. Across our cohorts, we found an average of 666.7404±45.1347 microspheres in the brain with a 4000-microsphere injection. All animals with less than 50 microspheres were excluded from microsphere quantification and localization analyses. It is likely these were unsuccessful/partial injections.

Although the mean number of recovered microspheres varied minimally across all cohorts, we found a significant difference between our aged non-diseased cohort and the young NTG cohort (Figure 5). It is important to note that our young and aged non-disease cohorts have less microspheres, which is likely a result of our initial injections being approximately 3000-3800 microspheres, prior to adjusting to an injection of 4000 microspheres for the remaining surgeries. This helps explain the discrepancy in the mean number of microspheres across experimental cohorts.

Our lab found microspheres in the heart and the lung of these mice, although this has not been further investigated at this point. It is possible the degree of lodged microspheres in peripheral organs may explain differences in total microspheres found in the brain (e.g. less

microspheres in the brain, but more in other organs or vice versa). Investigating microsphere load across organs may help further explain the variability across injections.

*4.2 Microspheres preferentially localized to the thalamus when accounting for region size*

Several studies have further characterized the distribution of microspheres across the brain regions. In agreement with current literature, we found that the neocortex accumulated more microspheres than any other region, followed by the thalamus and hippocampus (Figure 6)[23,29-32]. When the size of the region was accounted for, it was found that the thalamus had a greater number of microspheres per volume of brain region for all cohorts, which is in line with our previous study that determined the thalamus had the largest density of microspheres (Figure 7)[30].

In humans, microinfarcts are found in both subcortical and cortical regions, seemingly without preference[6]. Our mouse model produces stochastic distribution of microemboli across regions, however, it has previously been found that not all lodged microspheres result in the formation of a microinfarct[23]. Silasi et al. found that the microspheres in the hippocampus and white matter were more likely to induce a microinfarct compared to microspheres in other brain regions[23]. In mice, the hippocampus and white matter has been found to have relatively lower capillary density, which could potentially explain the greater incidence of lodged microspheres producing injury[82-84]. Moreover, despite equivalent levels of resting oxygen consumption, one study found that the hippocampus exhibits lower resting blood flow compared to the V1 cortex, likely as a result of lower vascular density and flux in individual capillaries[84]. Aswell, it was found that the hippocampus had weaker neurovascular coupling compared to the V1 cortex with fewer and smaller local vessel dilations in response to increases in neuronal activity and an overall smaller increase in blood volume[84]. Taken together, the hippocampus is likely more susceptible to damage following impairment in blood flow as a result of decreased vessel density and an already lower resting blood flow.

*4.2 Angiophagy timeline in young cohort*

Previous studies have presented inconclusive timelines for the process of angiophagy, which may be explained by small sample sizes and the use of varying sizes and composition of microemboli. The currently literature uses rather small sample sizes, with as low as 40 and as high as 195 microemboli quantified per timepoint in total[38-39,41]. Additionally, two papers from the same group published just one year apart observe significantly different rates of angiophagy

for the same size and composition of microspheres (15um) with 76% extravasated at day 7 in their 2019 study and 33% extravasated at the same timepoint in their 2020 study[38-39]. Together, the present literature on the process of angiophagy fall short in thoroughly quantifying the process with adequate sample sizes and are unable to replicate findings. Our goal was to add to the literature on angiophagy with larger sample sizes, with 10-100 microspheres sampled per mouse, with 5-16 mice used at each timepoint. Moreover, the two groups that have previously quantified the timecourse of angiophagy use varying quantities and makeups of microemboli, thus it is important we establish our own timeline of angiophagy specific to our model.

Across these studies, different microemboli are injected of varying sizes which may contribute to discrepancies in the proposed angiophagy timelines. Our results show that approximately 17% of microspheres have extravasated from the vessel at the day 7 timepoint in young, non-diseased mice. This is in contrast to other studies, which suggest 78% or 58% of fibrin and cholesterol clots, respectively, or 76% of polystyrene microspheres extravasate by day 7[38,50]. Notably in these studies, the size range of the fibrin and cholesterol clots were 8-20$\mu$m, while the microspheres were 15$\mu$m[38,50]. It is possible that the size of the emboli plays a role in the rate of angiophagy, as smaller microemboli may be more easily engulfed by the endothelial cells and translocated into the surrounding parenchyma. This is especially relevant with fibrin clots which can be broken down into fragments by tPA prior to translocation[49]. The effects of size were shown by van der Wijk whereby 33% of 15$\mu$m microspheres extravasated by day 7, while only 18% of 25$\mu$m microspheres had undergone angiophagy at this same timepoint[39].

At day 14, we found that approximately 43% of microspheres had extravasated from the vessel (Figure 8). This is comparable to the first study on angiophagy published by Lam et al. citing that just over 45% of microspheres (10-15$\mu$m in diameter) had undergone extravasation at this time point[50].

Moreover, the composition of microemboli used in quantifying angiophagy may help explain the current discrepancies. Lam et al. found that the percent of emboli that had undergone extravasation was significantly different between fibrin clots and cholesterol clots at the day 2 timepoint, whereby nearly 5% of the fibrin clots had extravasated, while in contrast, just under 40% of the cholesterol clots had extravasated[50]. By the day 8 time point, fibrin clots reached just under 80% extravasation, while only 60% of cholesterol clots had extravasated[50]. Additionally, van Der Wijk et al. investigated how the process of angiophagy was impacted by the

composition of microemboli[45]. Angiophagy was quantified in rats following injection of 12$\mu$m microspheres made up of varying combinations of poly(ether ester urethane) multiblock copolymers. It was found the rate of angiophagy was in fact impacted by the microsphere composition, whereby at day 14, the rate of extravasation varied significantly between 3.3% and 20.7%[45].

Novel to our study, we were also interested in understanding if angiophagy occurred at varying rates in different brain regions, which could be an additional factor that could account for the noted discrepancies. Furthermore, because we are interested in investigating whether the number of microspheres brain wide plays a role in the efficiency of angiophagy, understanding if regions with more or less microspheres display differences in the rate of extravasation was of interest. For example, although not significant in every cohort, the thalamus had a greater number of microspheres per volume of region compared to the cortex, striatum and hippocampus across all cohorts (Figure 7). Moreover, this becomes especially important when investigating angiophagy in our AD mouse model where the hippocampus has significantly greater amyloid $\beta$ and tau load compared to the cortex[69]. In our study, we found there to be no significant difference in angiophagy across most experimental cohorts and timepoints (Figure 9-10, 12-15).

In conclusion, there appears to be inconsistencies in reported timelines of angiophagy, with no consensus on the timepoint at which a majority of microemboli are extravasated outside of the vessel. It is likely the size of the emboli in addition to emboli composition can help reconcile these discrepancies in the current literature. Defining a timecourse for angiophagy is important in understanding angiophagy as a potential protective mechanism of the brain and investigating the relationship between emboli extravasation and hypoxia, blood brain barrier disruption, immune response and the development of infarcted tissue. Moreover, if angiophagy were to be used as a therapeutic target, it would be beneficial to understand at what point the process is the most efficient. Expanding the timecourse beyond day 14 could also be of interest to investigate whether the process of angiophagy continues until all microspheres have extravasated, as van der Wijk observed at day 28, or if its efficiency reaches a plateau[38].

*4.3 Delayed angiophagy in aged cohort*

Previously, Lam et al. studied the effects of aging on the process of angiophagy and found that clot (fibrin and cholesterol) extravasation decreased by just over 20% at day 4 and

microsphere (polystyrene) extravasation decreased markedly by just over 30% at day 14 in 22-month-old mice compared to 4-month-old[50].

We present similar findings in 9–20-month-old mice whereby at day 14, microsphere extravasation decreased by just over 30% as a result of aging, from 43.9% in young mice to 10.6% in aged mice (Figure 8). The effects of aging on the rate of angiophagy appear to be more prominent at this later timepoint, as microsphere extravasation decreased by merely 8.5% at day 3 and 10% at day 7, approximately (Figure 8). While the percent of extravasated microspheres jumps 36% between day 7 and 14 (from 17% to 43%) in young mice, extravasated microspheres only increase by 4% between day 7 and 14 (from 7% to 11%) in aged mice, approximately (Figure 8). If angiophagy does hit a plateau, it may be the case that aged animals reach their peak of angiophagy efficiency earlier than young animals, hence the diminished increase in extravasated microspheres between time points in aged animals.

In humans, it has been found that microinfarcts are present in 24% of those aged 75 years and older not associated with forms of dementia[3]. It is likely that vascular alterations seen in aging play a role in the observed decrease in the rate of angiophagy. For example, it is possible an increase in basal lamina thickness and collagen deposition, along with arterial stiffening caused by a decrease in elastin expression, make it more difficult for endothelial remodeling to occur and subsequently the engulfment and translocation of microemboli[50,52].

### *4.4 Prior to onset of AD pathology, minimal increase in angiophagy efficiency observed in 3xTg mice compared to non-transgenic controls*

Microinfarcts are commonly observed in those with Alzheimer's disease, presenting in 43% of AD patients[3]. Several vascular changes are seen in AD, such as hypoperfusion and overall decrease in vessel density[56]. We hypothesize that some of these vascular changes, such as arterial stiffening due to CAA, may impair this process of angiophagy[66]. To test our hypothesis, we used a 3xTg mouse model of AD. The few studies that have looked at vascular alterations in this mouse model have found 3xTg mice have decreased arterial flow, decreased density of penetrating arterioles, and importantly for studying angiophagy, vascular amyloid $\beta$ accumulation and thickened basement membrane, which may impact endothelial remodeling[69-71]. Notably, most of these vascular changes occur in older 3xTg mice beyond 11 months, which is why we chose to compare angiophagy in 4-6 month mice and 12-14 month mice for our study.

We found that the rate of angiophagy was generally comparable between the NTG and 3xTg cohorts at the earlier timepoint (day 3) and differences arose at day 7 and 14. Angiophagy followed the same trend as young, non-diseased mice whereby extravasation increased over 14 days. At day 3, 97% and 96% of microspheres were obstructing the vessels in the NTG and 3xTg cohorts, respectively. By day 14, 43% of microspheres extravasated from the vessel in the NTG cohort, compared to 47% in the 3xTg cohort.

Since severe AD pathology and vascular differences are likely not present at this timepoint (2-5 months) based on previous literature, we expected the rate of angiophagy to be comparable between NTG and 3xTg mice. Although not significant, we do see a general trend at day 14 whereby 3xTg mice have less obstructing microspheres and more microspheres in the going out and extravasated stages compared to NTG mice.

A possible explanation for this is the hypothesized role of matrix metalloproteinases in the process of angiophagy. Gelatinases A (MMP2) and B (MMP9) are commonly studied in the brain and contribute to remodeling of basal lamina and other processes like angiogenesis and apoptosis[85]. Moreover, they play a role in the disruption of blood brain barrier, whereby MMP-mediated BBB disruption is a result of MMPs attacking the extracellular matrix, basal lamina and tight junctions of endothelial cells[85-76]. In studying angiophagy, Lam et al. found increased gelatinolytic activity at sites of occluded vessels compared to unoccluded vessels, significantly at day 7 in the microsphere embolus model, and a decrease in angiophagy with the addition of a MMP2/9 inhibitor[50]. This points to the possibility that MMPs play a role in angiophagy. MMPs have been found to increase in levels in response to ischemic injury, therefore it is likely that MMP levels increase in response to microvessel occlusion, thus facilitating the process of angiophagy [87].

Importantly, MMPs have also been implicated in Alzheimer's disease and facilitate the process of amyloid β clearance. Alzheimer's patients have an increase in expression of MMPs in brain tissue and plasma[88]. It has been found that MMPs are endogenously induced by amyloid molecules in blood vessels, astrocytes, and microglia[89]. Specifically, MMP9 has been found to degrade amyloid β peptides and amyloid β fibrils[89]. APP/PSEN1 transgenic mice have shown to have increased MMP2 and MMP9 concentrations in astrocytes around amyloid plaques[89]. In MMP2/9 KO mice, levels of steady state Aβ significantly increased[90].

Since the presence of amyloid β has been shown to induce expression of MMP2/9, it is possible that 3xTg mice display heightened levels of MMP2/9 activity, like in Alzheimer's patients. This could account for the decrease in microspheres obstructing vessels and increase in microspheres going out and extravasated in 3xTg mice compared to NTG mice. To further investigate this, gelatin zymography could be performed to identify if there is a global increase in MMP2/9 levels in 3xTg mice compared to NTG mice and moreover, if gelatinolytic activity is further increased at the sites of angiophagy in AD mice.

*4.5 Increased angiophagy efficiency observed in aged 3xTg mice compared to age-matched non-transgenic controls at day 7 and 14*

We initially hypothesized that Alzheimer's disease pathology in our aged AD mice would impair the process of angiophagy as a result of cerebral amyloid angiopathy and thickened basement membrane, and that these effects would be exacerbated in aged Alzheimer's mice when disease pathology is more severe. Interestingly, we found that 3xTg mice were more efficient at angiophagy whereby at day 7 and 14, significantly more microspheres were in the going out stage compared to the NTG mice. Moreover, although not significant, we observe the same trend of angiophagy efficiency at day 14 in aged 3xTg mice whereby less microspheres are obstructing vessels and more microspheres have extravasated compared to NTG mice.

ElAli et al. studied the relationship between microinfarcts and AD in APP/PS1 mice and found microinfarcts decreased amyloid pathology, including the number and volume of plaques and frequency of cerebral amyloid angiophagy, compared to sham mice (AD mice without micro-occlusions) 1-month post-surgery. They hypothesized that inducing vessel occlusions leads to the subsequent activation and recruitment of immune cells, including microglial and peripheral phagocytic immune cells, which may subsequently help clear amyloid β.

It is possible that amyloid pathology did not impair angiophagy in aged 3xTg mice like hypothesized because the recruitment of immune cells to sites of vessel occlusion promoted amyloid β clearance, thus limiting the impact amyloid β pathology has on the process of angiophagy. To further explore this avenue, it would be beneficial to investigate the effect of micro-occlusions on AD pathology in our 3xTg model and explore potential correlations between presence of amyloid β, immune cell recruitment/activation, and the rate of angiophagy.

Importantly, the hypothesis that microvessel occlusions recruit immune cells and subsequently aid in the clearance of amyloid pathology only explains why 3xTg mice would have similar levels of angiophagy compared to NTG mice. However, this does not explain our findings whereby 3xTg mice are more efficient at angiophagy at the day 14 time point. It is possible that MMPs also play a role in explaining this phenomenon. Higher levels of MMPs have been associated with late-stage Alzheimer's disease, so it may be the case that we see a more significant increase in the percent of microspheres in the going out stage in the aged 3xTg mice as a result of greater MMP expression at this age[91]. Performing gelatin zymography to quantify protease activity levels would be beneficial to explore this hypothesis. Furthermore, it would be of interest to extend the timeline beyond day 14 and investigate whether this difference in angiophagy efficiency between NTG and 3xTg mice becomes more apparent.

*4.6 Microsphere load weakly correlated with rate of angiophagy*

Previous studies investigating angiophagy have proposed varying timelines for this process. The papers have a few methodological differences that could explain this, such as studying this process using varying microemboli sizes (8-25um) or differing compositions (cholesterol vs fibrin vs polystyrene). Notably, the studies also used varying numbers of injected microemboli per surgery. Some studies used upwards of 31,125 microemboli per injection, while other studies used as low as 1500 microemboli[41,50].

Our goal was to understand if microsphere load is correlated with the rate of extravasation to understand if the number of microspheres present in the brain impacted the process of angiophagy. We assessed correlations for each cohort (young, aged, young NTG and 3xTg) at each time point (day 3, 7 and 14). The aged non-diseased cohort at day 3 was the only correlation found to have a significant relationship between the number of microspheres and the percent of extravasated microspheres with an r value of 0.8548. The remaining timepoints across cohorts revealed no significant relationships, although a general positive correlation trend was observed across most cohorts/timepoints indicating greater microsphere load is associated with greater occurrence of angiophagy. It is unlikely there is a true correlation between microsphere load and the percent of extravasation given the variability in correlations and lack of significant r values. As well, we have a rather low sample size for some time points and cohorts, so expanding the number of animals used could be beneficial in further investigating a potential relationship here.

## *5 Conclusion*

In conclusion, we have proposed a timeline of angiophagy whereby approximately 43% of microspheres have extravasated by day 14 in young mice. Moreover, this process is delayed in aged mice, with 80% of microspheres obstructing the vessel at day 14. In both young and aged Alzheimer's disease mice, we see limited differences in the rate of angiophagy between NTG and 3xTG mice until day 14, whereby we observe fewer microspheres obstructing vessels and more microspheres in the process of going out and extravasated in 3xTg mice compared to NTG mice. Taken together, it is possible that the process of angiophagy is impeded in aging, which may help explain the increased presence of microinfarcts in the aging clinical population. Conversely, due to the complex and heterogenous nature of AD, it is likely there is an alternate factor that more prominently contributes to the increased presence of microinfarcts in Alzheimer's patients, such as hypoperfusion, as angiophagy was found to be more efficient in our AD model compared to non-transgenic controls.

### *5.1 Significance and real-world application*

This study was the first to propose an extensive timeline of angiophagy in aged and Alzheimer's disease mice, while elaborating on the current angiophagy timelines in young, non-diseased rodents. Furthermore, we are the first to compare angiophagy in different brain regions, as well as investigate a potential correlation between microsphere load and the occurrence of angiophagy.

#### *5.1.1 Potential therapeutic targets*

Understanding the timecourse of angiophagy is important when considering potential therapeutic targets of the process. As per Grutzendler et al., the early stage of angiophagy is described as lamellipodia projections entrapping emboli and retaining them in place[49]. It is likely this stage prevents emboli washout and hinders the ability of fibrinolytic agents to degrade engulfed emboli. Being able to target the action of actin cytoskeleton to accelerate this process would be beneficial in promoting overall emboli clearance. The second stage of angiophagy occurs when the embolus is physically translocated outside the vessel[49]. It is possible that this phase could be enhanced by targeting the opening of the endothelial barrier, potentially through promoting MMP expression at sites of vessel occlusion.

### *5.1.2 Angiophagy and microplastics*

There is an ever-increasing concern of the effects of microplastics on human health, with greater accumulation in the brain than other organs. Microplastics have been associated with an increased risk of stroke and heart attack[92]. Notably, microplastics accumulated at a greater proportion in the brain of individuals with dementia diagnosis, primarily in cerebrovascular walls and immune cells[93]. How microplastics affect tissue integrity and cognitive function is still unknown. One study investigating the effects of microplastics in mice found microvessels were more susceptible to alterations in blood flow following occlusion, as well, vessel occlusion resulted in transient cognitive deficits[94]. Although not observed in humans, it is possible microplastics undergo this same process of angiophagy to resolve vessel perfusion. However, the effects of microplastics residing in the brain parenchyma and whether angiophagy would help preserve tissue integrity and subsequent cognitive decline is unknown.

### *5.1.3 Angiophagy and drug delivery*

Additionally, angiophagy has been proposed as a mechanism to bypass the blood brain barrier for drug delivery, a significant issue in the clinical realm as large molecules cannot be targeted directly to the brain. van der Wijk et al. studied angiophagy with biodegradable microspheres composed of poly(ether ester urethane) multi-block copolymers with differing combinations of lactide, glycolide, ε-caprolactone, dioxanone and polyethylene glycol, which determine factors important to drug release such as degradation, hydrophilicity, and drug release kinetics[45]. This study found different microsphere compositions extravasated at different rates, hinting at the importance of microsphere make-up in the timely delivery of the drugs if relying on angiophagy. Several limitations of this approach to drug delivery to the brain must be considered, including the invasive nature of the intra-arterial microsphere injection, the risk of development of microinfarcts as a result of ischemia, BBB leakage, or immune response. Moreover, angiophagy appears to be inefficient, with well under 50% of the microspheres extravasating from the vessel after 2 weeks, which needs to be taken into account when determining dose and time release of the drugs[45].

### *5.2 Limitations*

#### *5.2.1 Angiophagy quantification*

One limitation of our study is our method of angiophagy quantification. For this project, Evans Blue was primarily used for vascular labeling as it binds to albumin, although this dye is typically used to identify blood brain barrier disruption[95]. In previous studies that quantified angiophagy, an endothelial label was used, such as Tie-2 GFP or laminin, in addition to a vascular label. Without an endothelial label, it is more difficult to distinguish between the stages of angiophagy as vascular labelling may be incomplete in regions of non-perfusion as a result of vessel occlusion.

Moreover, it is possible that vessel degradation occurred with previously occluded vessels, and thus our quantification of extravasated microspheres is an overestimation. Previous studies have found that ischemia-related BBB breakdown occurs resulting in endothelial damage, including edema and ruptures of luminal cell membrane, and ultimately basement membrane degradation and endothelial cell death hours following stroke[96]. One way to account for vessel degradation would be quantification of angiophagy *in vivo*, which although time consuming, is likely more reliable than quantifying this dynamic process in static histological samples.

#### *5.2.2 Sex differences in 3xTg mice*

It is known that females have a greater risk of developing Alzheimer's disease, in addition to experiencing a more rapid cognitive decline following diagnosis[97]. A precise explanation to why females exhibit Alzheimer's at a rate of 2 to 1 is largely unknown, with factors such as differences in amyloid clearance, hormones, and immune response being explored[99]. 3xTg mice exhibit sex differences, namely it has been reported that female mice display earlier signs of amyloid β in serum and brain tissue which accelerates more rapidly than male counterparts[70,100-104]. Moreover, phosphorylated tau pathology appears to be more abundant in females beyond 12 months[79,103-104].

Our study used both male and female mice to study angiophagy. It is possible that the rate of angiophagy, although previously established as having no significant differences between sexes in young, non-diseased rodents, varies between female and male 3xTg mice as a result of the greater pathological burden in female mice[39]. Adding more animals to generate statistical

power for comparison of sexes would be an adequate way to assess potential effects of sex on angiophagy in 3xTg mice.

*5.3 Future directions*

In quantifying microsphere load in each brain sample, it was found that the number of microspheres differed measurably, ranging from a few beads to a thousand beads, despite maintaining the same concentration between injections. Microspheres were also observed in the heart and lungs but it is unclear how the microspheres reach these organs. Potentially they successfully circulate through the brain and only then become lodged in the heart and lungs or are backflushed immediately after injection when regular blood flow returns to the carotid artery. We are interested in quantifying bead load in these organs to understand how it relates to the number of microspheres in the brain (e.g. do less microspheres in the brain correlate with more microspheres in the heart/lungs or more microspheres in the brain correlate with more microspheres in the heart/lungs).

*References*


1. van Veluw, S. J., Shih, A. Y., Smith, E. E., Chen, C., Schneider, J. A., Wardlaw, J. M., Greenberg, S. M., & Biessels, G. J. (2017). Detection, risk factors, and functional consequences of cerebral microinfarcts. *Lancet Neurology*, *16*(9), 730–740. https://doi.org/10.1016/S1474-4422(17)30196-5
2. Westover MB, Bianchi MT, Yang C, Schneider JA, Greenberg SM. Estimating cerebral microinfarct burden from autopsy samples. Neurology 2013; 13: 1–5.
3. Corrada, M. M., Sonnen, J. A., Kim, R. C., & Kawas, C. H. (2016, August). *Microinfarcts are common and strongly related to dementia in the oldest-old: The 90+ study*. Alzheimer's & dementia : the journal of the Alzheimer's Association. https://www.ncbi.nlm.nih.gov/pmc/articles/PMC4980175/
4. Damasceno B. P. (2012). Relationship between cortical microinfarcts and cognitive impairment in Alzheimer's disease. *Dementia & neuropsychologia*, *6*(3), 131–136. https://doi.org/10.1590/S1980-57642012DN06030004
5. Arvanitakis Z, Leurgans SE, Barnes LL, Bennett DA, Schneider JA. Microinfarct pathology, dementia, and cognitive systems. Stroke. 2011;42:722–7. doi: 10.1161/STROKEAHA.110.595082
6. Brundel, M., de Bresser, J., van Dillen, J. J., Kappelle, L. J., & Biessels, G. J. (2012). Cerebral microinfarcts: a systematic review of neuropathological studies. *Journal of cerebral blood flow and metabolism : official journal of the International Society of Cerebral Blood Flow and Metabolism*, *32*(3), 425–436. https://doi.org/10.1038/jcbfm.2011.200
7. Yilmazer-Hanke, D., Mayer, T., Müller, HP. *et al.* Histological correlates of postmortem ultra-high-resolution single-section MRI in cortical cerebral microinfarcts. *acta neuropathol commun* 8, 33 (2020). https://doi.org/10.1186/s40478-020-00900-1
8. Brown W. R. (2010). A review of string vessels or collapsed, empty basement membrane tubes. Journal of Alzheimer's disease : JAD, 21(3), 725–739. https://doi.org/10.3233/JAD-2010-100219
9. Okamoto, Y., Ihara, M., Fujita, Y., Ito, H., Takahashi, R., & Tomimoto, H. (2009). Cortical microinfarcts in Alzheimer's disease and subcortical vascular

dementia. *Neuroreport*, *20*(11), 990–996. https://doi.org/10.1097/WNR.0b013e32832d2e6a

10. Arvanitakis, Z., Capuano, A. W., Leurgans, S. E., Buchman, A. S., Bennett, D. A., & Schneider, J. A. (2017). The Relationship of Cerebral Vessel Pathology to Brain Microinfarcts. *Brain pathology (Zurich, Switzerland)*, *27*(1), 77–85. https://doi.org/10.1111/bpa.12365
11. Arboix, A., Ferrer, I., & Martí-Vilalta, J. L. (1996). Análisis clínico-anatomopatológico de 25 pacientes con infartos lacunares [Clinico-anatomopathologic analysis of 25 patients with lacunar infarction]. *Revista clinica espanola*, *196*(6), 370–374.
12. Kövari, E., Herrmann, F. R., Gold, G., Hof, P. R., & Charidimou, A. (2017). Association of cortical microinfarcts and cerebral small vessel pathology in the ageing brain. *Neuropathology and applied neurobiology*, *43*(6), 505–513. https://doi.org/10.1111/nan.12366
13. van Veluw, S. J., Hilal, S., Kuijf, H. J., Ikram, M. K., Xin, X., Yeow, T. B., Venketasubramanian, N., Biessels, G. J., & Chen, C. (2015). Cortical microinfarcts on 3T MRI: Clinical correlates in memory-clinic patients. *Alzheimer's & dementia : the journal of the Alzheimer's Association*, *11*(12), 1500–1509. https://doi.org/10.1016/j.jalz.2014.12.010
14. Bernick, C., Kuller, L., Dulberg, C., Longstreth, W. T., Jr, Manolio, T., Beauchamp, N., Price, T., & Cardiovascular Health Study Collaborative Reseach Group (2001). Silent MRI infarcts and the risk of future stroke: the cardiovascular health study. *Neurology*, *57*(7), 1222–1229. https://doi.org/10.1212/wnl.57.7.1222
15. Hilal S, Chai YL, van Veluw S, et al. Association Between Subclinical Cardiac Biomarkers and Clinically Manifest Cardiac Diseases With Cortical Cerebral Microinfarcts. *JAMA Neurol.* 2017;74(4):403–410. doi:10.1001/jamaneurol.2016.5335
16. Troncoso, J. C., Zonderman, A. B., Resnick, S. M., Crain, B., Pletnikova, O., & O'Brien, R. J. (2008). Effect of infarcts on dementia in the Baltimore longitudinal study of aging. *Annals of neurology*, *64*(2), 168–176. https://doi.org/10.1002/ana.21413
17. Del Ser, T., Hachinski, V., Merskey, H., & Munoz, D. G. (2005). Alzheimer's disease with and without cerebral infarcts. *Journal of the neurological sciences*, *231*(1-2), 3–11. https://doi.org/10.1016/j.jns.2004.08.016

18. Lee, C. S., Larson, E. B., Gibbons, L. E., Latimer, C. S., Rose, S. E., Hellstern, L. L., Keene, C. D., Crane, P. K., & Adult Changes in Thought (ACT) Study (2019). Ophthalmology-Based Neuropathology Risk Factors: Diabetic Retinopathy is Associated with Deep Microinfarcts in a Community-Based Autopsy Study. *Journal of Alzheimer's disease : JAD*, *68*(2), 647–655. https://doi.org/10.3233/JAD-181087
19. Wang, L. Y., Larson, E. B., Sonnen, J. A., Shofer, J. B., McCormick, W., Bowen, J. D., Montine, T. J., & Li, G. (2009). Blood pressure and brain injury in older adults: findings from a community-based autopsy study. *Journal of the American Geriatrics Society*, *57*(11), 1975–1981. https://doi.org/10.1111/j.1532-5415.2009.02493.x
20. Arvanitakis, Z., Leurgans, S. E., Barnes, L. L., Bennett, D. A., & Schneider, J. A. (2011). Microinfarct pathology, dementia, and cognitive systems. *Stroke*, *42*(3), 722–727. https://doi.org/10.1161/STROKEAHA.110.595082
21. Shih, A., Blinder, P., Tsai, P. *et al.* The smallest stroke: occlusion of one penetrating vessel leads to infarction and a cognitive deficit. *Nat Neurosci* 16, 55–63 (2013). https://doi.org/10.1038/nn.3278
22. Hall, C. N., Reynell, C., Gesslein, B., Hamilton, N. B., Mishra, A., Sutherland, B. A., O'Farrell, F. M., Buchan, A. M., Lauritzen, M., & Attwell, D. (2014). Capillary pericytes regulate cerebral blood flow in health and disease. *Nature*, *508*(7494), 55–60. https://doi.org/10.1038/nature13165
23. Silasi, G., She, J., Boyd, J. D., Xue, S., & Murphy, T. H. (2015). A mouse model of small-vessel disease that produces brain-wide-identified microocclusions and regionally selective neuronal injury. *Journal of cerebral blood flow and metabolism : official journal of the International Society of Cerebral Blood Flow and Metabolism*, *35*(5), 734–738. https://doi.org/10.1038/jcbfm.2015.8
24. Shih, A. Y., Nishimura, N., Nguyen, J., Friedman, B., Lyden, P. D., Schaffer, C. B., & Kleinfeld, D. (2013). Optically induced occlusion of single blood vessels in rodent neocortex. *Cold Spring Harbor protocols*, *2013*(12), 1153–1160. https://doi.org/10.1101/pdb.prot079509
25. Summers, P. M., Hartmann, D. A., Hui, E. S., Nie, X., Deardorff, R. L., McKinnon, E. T., Helpern, J. A., Jensen, J. H., & Shih, A. Y. (2017). Functional deficits induced by cortical microinfarcts. Journal of cerebral blood flow and metabolism : official journal of

the International Society of Cerebral Blood Flow and Metabolism, 37(11), 3599–3614. https://doi.org/10.1177/0271678X16685573

26. Wong Zhang, D. E., Zhang, S. R., Kim, H. A., Sobey, C. G., & De Silva, T. M. (2024). The Photothrombotic Model of Ischemic Stroke. *Methods in molecular biology (Clifton, N.J.)*, *2746*, 225–235. https://doi.org/10.1007/978-1-0716-3585-8_18
27. Huang, Y., Wu, Z., Lui, H., Zhao, J., Xie, S., & Zeng, H. (2019). Precise closure of single blood vessels via multiphoton absorption-based photothermolysis. Science advances, 5(5), eaan9388. https://doi.org/10.1126/sciadv.aan9388
28. Shih, A. Y., Hyacinth, H. I., Hartmann, D. A., & van Veluw, S. J. (2018). Rodent Models of Cerebral Microinfarct and Microhemorrhage. *Stroke*, *49*(3), 803–810. https://doi.org/10.1161/STROKEAHA.117.016995
29. Shen, Y., Cui, J., Zhang, S., Wang, Y., Wang, J., Su, Y., Xu, D., Liu, Y., Guo, Y., & Bai, W. (2022). Temporal alteration of microglia to microinfarcts in rat brain induced by the vascular occlusion with fluorescent microspheres. Frontiers in cellular neuroscience, 16, 956342. https://doi.org/10.3389/fncel.2022.956342
30. McDonald, M. W., Jeffers, M. S., Filadelfi, M., Vicencio, A., Heidenreich, G., Wu, J., & Silasi, G. (2021). Localizing Microemboli within the Rodent Brain through Block-Face Imaging and Atlas Registration. *eNeuro*, *8*(4), ENEURO.0216-21.2021. https://doi.org/10.1523/ENEURO.0216-21.2021
31. Shen, Y., Yao, M. J., Su, Y. X., Xu, D. S., Wang, J., Wang, G. R., Cui, J. J., Zhang, J. L., & Bai, W. Z. (2022). Histochemistry of microinfarcts in the mouse brain after injection of fluorescent microspheres into the common carotid artery. *Neural regeneration research*, *17*(4), 832–837. https://doi.org/10.4103/1673-5374.322470
32. Heiser H, Kiessler F, Roggenbach A, Ibanez I, Wieckhorst M, Helmchen F, Ggorgjieva J, Wahl A. Brain-wide microstrokes affect the stability of memory circuits in the hippocampus. bioRxiv 2024;612757. doi: https://doi.org/10.1101/2024.09.17.612757
33. Balbi, M., Vanni, M. P., Vega, M. J., Silasi, G., Sekino, Y., Boyd, J. D., LeDue, J. M., & Murphy, T. H. (2019). Longitudinal monitoring of mesoscopic cortical activity in a mouse model of microinfarcts reveals dissociations with behavioral and motor function. Journal of cerebral blood flow and metabolism : official journal of the International

Society of Cerebral Blood Flow and Metabolism, 39(8), 1486–1500. https://doi.org/10.1177/0271678X18763428

34. Holland PR, Searcy JL, Salvadores N, Scullion G, Chen G, Lawson G, et al. Gliovascular disruption and cognitive deficits in a mouse model with features of small vessel disease. Journal of Cerebral Blood Flow & Metabolism. 2015;35:1005–1014. doi: 10.1038/jcbfm.2015.12.
35. Okamoto Y, Yamamoto T, Kalaria RN, Senzaki H, Maki T, Hase Y, et al. Cerebral hypoperfusion accelerates cerebral amyloid angiopathy and promotes cortical microinfarcts. Acta Neuropathologica. 2012;123:381–394. doi: 10.1007/s00401-011-0925-9.
36. Lee ES, Yoon JH, Choi J, Andika FR, Lee T, Jeong Y. A mouse model of subcortical vascular dementia reflecting degeneration of cerebral white matter and microcirculation. Journal of Cerebral Blood Flow & Metabolism. 2017 doi: 10.1177/0271678X17736963.
37. Qiu, Y. M., Zhang, C. L., Chen, A. Q., Wang, H. L., Zhou, Y. F., Li, Y. N., & Hu, B. (2021). Immune Cells in the BBB Disruption After Acute Ischemic Stroke: Targets for Immune Therapy?. *Frontiers in immunology*, *12*, 678744. https://doi.org/10.3389/fimmu.2021.678744
38. van der Wijk, A. E., Lachkar, N., de Vos, J., Grootemaat, A. E., van der Wel, N. N., Hordijk, P. L., Bakker, E. N. T. P., & vanBavel, E. (2019). Extravasation of Microspheres in a Rat Model of Silent Brain Infarcts. *Stroke*, *50*(6), 1590–1594. https://doi.org/10.1161/STROKEAHA.119.024975
39. van der Wijk, AE., Georgakopoulou, T., Majolée, J. *et al.* Microembolus clearance through angiophagy is an auxiliary mechanism preserving tissue perfusion in the rat brain. *acta neuropathol commun* 8, 195 (2020). https://doi.org/10.1186/s40478-020-01071-9
40. Georgakopoulou, T., van der Wijk, A. E., Bakker, E. N. T. P., vanBavel, E., & INSIST investigators (2021). Recovery of Hypoxic Regions in a Rat Model of Microembolism. *Journal of stroke and cerebrovascular diseases : the official journal of National Stroke Association*, *30*(6), 105739. https://doi.org/10.1016/j.jstrokecerebrovasdis.2021.105739

41. Georgakopoulou, T., van der Wijk, A. E., van Bavel, E., & Bakker, E. N. T. P. (2023). Perivascular clearance of blood proteins after blood-brain barrier disruption in a rat model of microinfarcts. *Microvascular research*, *148*, 104515. https://doi.org/10.1016/j.mvr.2023.104515
42. Grutzendler J. (2013). Angiophagy: mechanism of microvascular recanalization independent of the fibrinolytic system. *Stroke*, *44*(6 Suppl 1), S84–S86. https://doi.org/10.1161/STROKEAHA.112.678730
43. Atochin, D. N., Murciano, J. C., Gürsoy-Ozdemir, Y., Krasik, T., Noda, F., Ayata, C., Dunn, A. K., Moskowitz, M. A., Huang, P. L., & Muzykantov, V. R. (2004). Mouse model of microembolic stroke and reperfusion. *Stroke*, *35*(9), 2177–2182. https://doi.org/10.1161/01.STR.0000137412.35700.0e
44. National Institute of Neurological Disorders and Stroke rt-PA Stroke Study Group (1995). Tissue plasminogen activator for acute ischemic stroke. *The New England journal of medicine*, *333*(24), 1581–1587. https://doi.org/10.1056/NEJM199512143332401
45. van der Wijk, A. E., Georgakopoulou, T., Steendam, R., Zuidema, J., Hordijk, P. L., Bakker, E. N. T. P., & van Bavel, E. (2023). Extravasation of biodegradable microspheres in the rat brain. *Drug Delivery*, *30*(1). https://doi.org/10.1080/10717544.2023.2194579
46. Smith, E. E., Schneider, J. A., Wardlaw, J. M., & Greenberg, S. M. (2012). Cerebral microinfarcts: the invisible lesions. *The Lancet. Neurology*, *11*(3), 272–282. https://doi.org/10.1016/S1474-4422(11)70307-6
47. Austin BP, Nair VA, Meier TB, Xu G, Rowley HA, Carlsson CM, Johnson SC, Prabhakaran V. Effects of hypoperfusion in Alzheimer's disease. J Alzheimers Dis. 2011;26 Suppl 3(Suppl 3):123-33. doi: 10.3233/JAD-2011-0010. PMID: 21971457; PMCID: PMC3303148.
48. Rapp, J. H., Pan, X. M., Sharp, F. R., Shah, D. M., Wille, G. A., Velez, P. M., Troyer, A., Higashida, R. T., & Saloner, D. (2000). Atheroemboli to the brain: size threshold for causing acute neuronal cell death. *Journal of vascular surgery*, *32*(1), 68–76. https://doi.org/10.1067/mva.2000.107315

49. Grutzendler, J., Murikinati, S., Hiner, B., Ji, L., Lam, C. K., Yoo, T., Gupta, S., Hafler, B. P., Adelman, R. A., Yuan, P., & Rodriguez, G. (2014). Angiophagy prevents early embolus washout but recanalizes microvessels through embolus extravasation. *Science translational medicine*, *6*(226), 226ra31. https://doi.org/10.1126/scitranslmed.3006585
50. Lam, C. K., Yoo, T., Hiner, B., Liu, Z., & Grutzendler, J. (2010). Embolus extravasation is an alternative mechanism for cerebral microvascular recanalization. *Nature*, *465*(7297), 478–482. https://doi.org/10.1038/nature09001
51. Iadecola C. (2014). Angiophagy: clearing or clogging microvessels?. *Science translational medicine*, *6*(226), 226fs10. https://doi.org/10.1126/scitranslmed.3008667
52. Peters R. (2006). Ageing and the brain. *Postgraduate medical journal*, *82*(964), 84–88. https://doi.org/10.1136/pgmj.2005.036665
53. Fonck, E., Feigl, G. G., Fasel, J., Sage, D., Unser, M., Rüfenacht, D. A., & Stergiopulos, N. (2009). Effect of aging on elastin functionality in human cerebral arteries. *Stroke*, *40*(7),2552–2556. https://doi.org/10.1161/STROKEAHA.108.528091
54. Erdő, F., Denes, L., & de Lange, E. (2017). Age-associated physiological and pathological changes at the blood-brain barrier: A review. *Journal of cerebral blood flow and metabolism : official journal of the International Society of Cerebral Blood Flow and Metabolism*, *37*(1), 4–24. https://doi.org/10.1177/0271678X16679420
55. Gleerup, G., & Winther, K. (1995). The effect of ageing on platelet function and fibrinolytic activity. *Angiology*, *46*(8), 715–718. https://doi.org/10.1177/000331979504600810
56. Thomasina L. Bailey, Claire B. Rivara, Anne B. Rocher & Patrick R. Hof (2004) The nature and effects of cortical microvascular pathology in aging and Alzheimer's disease, Neurological Research, 26:5, 573-578, DOI: 10.1179/016164104225016272
57. Rius-Pérez, S., Tormos, A. M., Pérez, S., & Taléns-Visconti, R. (2018). Vascular pathology: Cause or effect in alzheimer disease? *Neurología (English Edition)*, *33*(2), 112–120. https://doi.org/10.1016/j.nrleng.2015.07.008
58. Peers, C., Dallas, M. L., Boycott, H. E., Scragg, J. L., Pearson, H. A., & Boyle, J. P. (2009). Hypoxia and neurodegeneration. *Annals of the New York Academy of Sciences*, *1177*, 169–177. https://doi.org/10.1111/j.1749-6632.2009.05026.x

59. Hof, P. R., Bussière, T., Gold, G., Kövari, E., Giannakopoulos, P., Bouras, C., Perl, D. P., & Morrison, J. H. (2003). Stereologic evidence for persistence of viable neurons in layer II of the entorhinal cortex and the CA1 field in Alzheimer disease. *Journal of neuropathology and experimental neurology*, *62*(1), 55–67. https://doi.org/10.1093/jnen/62.1.55
60. Bussière, T., Gold, G., Kövari, E., Giannakopoulos, P., Bouras, C., Perl, D. P., Morrison, J. H., & Hof, P. R. (2003). Stereologic analysis of neurofibrillary tangle formation in prefrontal cortex area 9 in aging and Alzheimer's disease. *Neuroscience*, *117*(3), 577–592. https://doi.org/10.1016/s0306-4522(02)00942-9
61. Suter OC, Sunthorn T, Kraftsik R, Straubel J, Darekar P, Khalili K, et al. Cerebral hypoperfusion generates cortical watershed microinfarcts in Alzheimer disease. Stroke 2002; 33:1986–1992
62. Hays, C. C., Zlatar, Z. Z., & Wierenga, C. E. (2016). The Utility of Cerebral Blood Flow as a Biomarker of Preclinical Alzheimer's Disease. *Cellular and molecular neurobiology*, *36*(2), 167–179. https://doi.org/10.1007/s10571-015-0261-z
63. Binnewijzend, M. A., Benedictus, M. R., Kuijer, J. P., van der Flier, W. M., Teunissen, C. E., Prins, N. D., Wattjes, M. P., van Berckel, B. N., Scheltens, P., & Barkhof, F. (2016). Cerebral perfusion in the predementia stages of Alzheimer's disease. *European radiology*, *26*(2), 506–514. https://doi.org/10.1007/s00330-015-3834-9
64. Biffi, A., & Greenberg, S. M. (2011). Cerebral amyloid angiopathy: a systematic review. *Journal of clinical neurology (Seoul, Korea)*, *7*(1), 1–9. https://doi.org/10.3988/jcn.2011.7.1.1
65. Ventura-Antunes, L., Nackenoff, A., Romero-Fernandez, W., Bosworth, A. M., Prusky, A., Wang, E., Carvajal-Tapia, C., Shostak, A., Harmsen, H., Mobley, B., Maldonado, J., Solopova, E., Caleb Snider, J., David Merryman, W., Lippmann, E. S., & Schrag, M. (2024). Arteriolar degeneration and stiffness in cerebral amyloid angiopathy are linked to β-amyloid deposition and lysyl oxidase. bioRxiv : the preprint server for biology, 2024.03.08.583563. https://doi.org/10.1101/2024.03.08.583563
66. Zenaro, E., Piacentino, G., & Constantin, G. (2017). The blood-brain barrier in Alzheimer's disease. *Neurobiology of disease*, *107*, 41–56. https://doi.org/10.1016/j.nbd.2016.07.007

67. Wang Z, Wu D, Vinters HV. Hypoxia and reoxygenation of brain microvascular smooth muscle cells in vitro: cellular responses and expression of cerebral amyloid angiopathy-associated proteins. *APMIS.* 2002;110:423–434. doi: 10.1034/j.1600-0463.2002.100509.x
68. Oddo, S., Caccamo, A., Shepherd, J. D., Murphy, M. P., Golde, T. E., Kayed, R., Metherate, R., Mattson, M. P., Akbari, Y., & LaFerla, F. M. (2003). Triple-transgenic model of Alzheimer's disease with plaques and tangles: intracellular Abeta and synaptic dysfunction. *Neuron*, *39*(3), 409–421. https://doi.org/10.1016/s0896-6273(03)00434-3
69. Javonillo DI, Tran KM, Phan J, Hingco E, Kramár EA, da Cunha C, Forner S, Kawauchi S, Milinkeviciute G, Gomez-Arboledas A, Neumann J, Banh CE, Huynh M, Matheos DP, Rezaie N, Alcantara JA, Mortazavi A, Wood MA, Tenner AJ, MacGregor GR, Green KN, LaFerla FM. Systematic Phenotyping and Characterization of the 3xTg-AD Mouse Model of Alzheimer's Disease. Front Neurosci. 2022 Jan 24;15:785276. doi: 10.3389/fnins.2021.785276. PMID: 35140584; PMCID: PMC8818877.
70. Walek, K.W., Stefan, S., Lee, JH. *et al.* Near-lifespan longitudinal tracking of brain microvascular morphology, topology, and flow in male mice. *Nat Commun* 14, 2982 (2023). https://doi.org/10.1038/s41467-023-38609-z
71. Bourasset, F., Ouellet, M., Tremblay, C., Julien, C., Do, T. M., Oddo, S., LaFerla, F., & Calon, F. (2009). Reduction of the cerebrovascular volume in a transgenic mouse model of Alzheimer's disease. *Neuropharmacology*, *56*(4), 808–813. https://doi.org/10.1016/j.neuropharm.2009.01.006
72. Andrade-Guerrero, J., Orta-Salazar, E., Salinas-Lara, C., Sánchez-Garibay, C., Rodríguez-Hernández, L. D., Vargas-Rodríguez, I., Barron-Leon, N., Ledesma-Alonso, C., Diaz-Cintra, S., & Soto-Rojas, L. O. (2023). Effects of Voluntary Physical Exercise on the Neurovascular Unit in a Mouse Model of Alzheimer's Disease. *International Journal of Molecular Sciences*, *24*(13), 11134. https://doi.org/10.3390/ijms241311134
73. Quintana, D. D., Anantula, Y., Garcia, J. A., Engler-Chiurazzi, E. B., Sarkar, S. N., Corbin, D. R., Brown, C. M., & Simpkins, J. W. (2021). Microvascular degeneration occurs before plaque onset and progresses with age in 3xTg AD mice. *Neurobiology of aging*, *105*, 115–128. https://doi.org/10.1016/j.neurobiolaging.2021.04.019
74. Salvadores, N., Searcy, J. L., Holland, P. R., & Horsburgh, K. (2017). Chronic cerebral hypoperfusion alters amyloid-β peptide pools leading to cerebral amyloid angiopathy,

microinfarcts and haemorrhages in Tg-SwDI mice. Clinical science (London, England : 1979), 131(16), 2109–2123. https://doi.org/10.1042/CS20170962

75. Garcia-Alloza, M., Gregory, J., Kuchibhotla, K. V., Fine, S., Wei, Y., Ayata, C., Frosch, M. P., Greenberg, S. M., & Bacskai, B. J. (2011). Cerebrovascular lesions induce transient β-amyloid deposition. *Brain : a journal of neurology*, *134*(Pt 12), 3697–3707. https://doi.org/10.1093/brain/awr300
76. Venkat, P., Chopp, M., Zacharek, A., Cui, C., Zhang, L., Li, Q., Lu, M., Zhang, T., Liu, A., & Chen, J. (2017). White matter damage and glymphatic dysfunction in a model of vascular dementia in rats with no prior vascular pathologies. Neurobiology of aging, 50, 96–106. https://doi.org/10.1016/j.neurobiolaging.2016.11.002
77. Wang, M., Ding, F., Deng, S., Guo, X., Wang, W., Iliff, J. J., & Nedergaard, M. (2017). Focal Solute Trapping and Global Glymphatic Pathway Impairment in a Murine Model of Multiple Microinfarcts. The Journal of neuroscience : the official journal of the Society for Neuroscience, 37(11), 2870–2877. https://doi.org/10.1523/JNEUROSCI.2112-16.2017
78. Lecordier, S., Pons, V., Rivest, S., & ElAli, A. (2022). Multifocal Cerebral Microinfarcts Modulate Early Alzheimer's Disease Pathology in a Sex-Dependent Manner. *Frontiers in immunology*, *12*, 813536. https://doi.org/10.3389/fimmu.2021.813536
79. Kaiser, T., & Feng, G. (2019). Tmem119-EGFP and Tmem119-CreERT2 Transgenic Mice for Labeling and Manipulating Microglia. *eNeuro*, *6*(4), ENEURO.0448-18.2019. https://doi.org/10.1523/ENEURO.0448-18.2019
80. G. Nagel, T. Szellas, W. Huhn, S. Kateriya, N. Adeishvili, P. Berthold, D. Ollig, P. Hegemann, E. Bamberg, Channelrhodopsin-2, a directly light-gated cation-selective membrane channel, Proc. Natl. Acad. Sci. U.S.A. 100 (24) 13940-13945, https://doi.org/10.1073/pnas.1936192100 (2003).
81. Yates, S. C., Groeneboom, N. E., Coello, C., Lichtenthaler, S. F., Kuhn, P. H., Demuth, H. U., Hartlage-Rübsamen, M., Roßner, S., Leergaard, T., Kreshuk, A., Puchades, M. A., & Bjaalie, J. G. (2019). QUINT: Workflow for Quantification and Spatial Analysis of Features in Histological Images From Rodent Brain. *Frontiers in neuroinformatics*, *13*, 75. https://doi.org/10.3389/fninf.2019.00075

82. Cavaglia, M., Dombrowski, S. M., Drazba, J., Vasanji, A., Bokesch, P. M., & Janigro, D. (2001). Regional variation in brain capillary density and vascular response to ischemia. *Brain research*, *910*(1-2), 81–93. https://doi.org/10.1016/s0006-8993(01)02637-3
83. Xiong, B., Li, A., Lou, Y., Chen, S., Long, B., Peng, J., Yang, Z., Xu, T., Yang, X., Li, X., Jiang, T., Luo, Q., & Gong, H. (2017). Precise Cerebral Vascular Atlas in Stereotaxic Coordinates of Whole Mouse Brain. *Frontiers in neuroanatomy*, *11*, 128. https://doi.org/10.3389/fnana.2017.00128
84. Shaw, K., Bell, L., Boyd, K. et al. Neurovascular coupling and oxygenation are decreased in hippocampus compared to neocortex because of microvascular differences. Nat Commun 12, 3190 (2021). https://doi.org/10.1038/s41467-021-23508-y
85. Rosenberg G. A. (2009). Matrix metalloproteinases and their multiple roles in neurodegenerative diseases. The Lancet. Neurology, 8(2), 205–216. https://doi.org/10.1016/S1474-4422(09)70016-X
86. Rempe, R. G., Hartz, A. M. S., & Bauer, B. (2016). Matrix metalloproteinases in the brain and blood-brain barrier: Versatile breakers and makers. *Journal of cerebral blood flow and metabolism : official journal of the International Society of Cerebral Blood Flow and Metabolism*, *36*(9), 1481–1507. https://doi.org/10.1177/0271678X16655551
87. Asahi, M., Wang, X., Mori, T., Sumii, T., Jung, J. C., Moskowitz, M. A., Fini, M. E., & Lo, E. H. (2001). Effects of matrix metalloproteinase-9 gene knock-out on the proteolysis of blood-brain barrier and white matter components after cerebral ischemia. The Journal of neuroscience : the official journal of the Society for Neuroscience, 21(19), 7724–7732. https://doi.org/10.1523/JNEUROSCI.21-19-07724.2001
88. Lorenzl, S., Albers, D. S., Relkin, N., Ngyuen, T., Hilgenberg, S. L., Chirichigno, J., Cudkowicz, M. E., & Beal, M. F. (2003). Increased plasma levels of matrix metalloproteinase-9 in patients with Alzheimer's disease. Neurochemistry international, 43(3), 191–196. https://doi.org/10.1016/s0197-0186(03)00004-4
89. Yan, P., Hu, X., Song, H., Yin, K., Bateman, R. J., Cirrito, J. R., Xiao, Q., Hsu, F. F., Turk, J. W., Xu, J., Hsu, C. Y., Holtzman, D. M., & Lee, J. M. (2006). Matrix metalloproteinase-9 degrades amyloid-beta fibrils in vitro and compact plaques in situ.

The Journal of biological chemistry, 281(34), 24566–24574. https://doi.org/10.1074/jbc.M602440200

90. Yin, K. J., Cirrito, J. R., Yan, P., Hu, X., Xiao, Q., Pan, X., Bateman, R., Song, H., Hsu, F. F., Turk, J., Xu, J., Hsu, C. Y., Mills, J. C., Holtzman, D. M., & Lee, J. M. (2006). Matrix metalloproteinases expressed by astrocytes mediate extracellular amyloid-beta peptide catabolism. The Journal of neuroscience : the official journal of the Society for Neuroscience, 26(43), 10939–10948. https://doi.org/10.1523/JNEUROSCI.2085-06.2006
91. Hernandes-Alejandro, M., Montaño, S., Harrington, C. R., Wischik, C. M., Salas-Casas, A., Cortes-Reynosa, P., Pérez Salazar, E., Cazares-Apatiga, J., Apatiga-Perez, R., Ontiveros Torres, M. Á., Perry, G., Pacheco-Herrero, M., & Luna-Muñoz, J. (2020). Analysis of the Relationship Between Metalloprotease-9 and Tau Protein in Alzheimer's Disease. Journal of Alzheimer's disease : JAD, 76(2), 553–569. https://doi.org/10.3233/JAD-200146mb
92. Marfella, R., Prattichizzo, F., Sardu, C., Fulgenzi, G., Graciotti, L., Spadoni, T., D'Onofrio, N., Scisciola, L., La Grotta, R., Frigé, C., Pellegrini, V., Municinò, M., Siniscalchi, M., Spinetti, F., Vigliotti, G., Vecchione, C., Carrizzo, A., Accarino, G., Squillante, A., Spaziano, G., … Paolisso, G. (2024). Microplastics and Nanoplastics in Atheromas and Cardiovascular Events. The New England journal of medicine, 390(10), 900–910. https://doi.org/10.1056/NEJMoa2309822
93. Marfella, R., Prattichizzo, F., Sardu, C., Fulgenzi, G., Graciotti, L., Spadoni, T., D'Onofrio, N., Scisciola, L., La Grotta, R., Frigé, C., Pellegrini, V., Municinò, M., Siniscalchi, M., Spinetti, F., Vigliotti, G., Vecchione, C., Carrizzo, A., Accarino, G., Squillante, A., Spaziano, G., … Paolisso, G. (2024). Microplastics and Nanoplastics in Atheromas and Cardiovascular Events. The New England journal of medicine, 390(10), 900–910. https://doi.org/10.1056/NEJMoa2309822
94. Huang, H., Hou, J., Li, M., Wei, F., Liao, Y., & Xi, B. (2025). Microplastics in the bloodstream can induce cerebral thrombosis by causing cell obstruction and lead to neurobehavioral abnormalities. Science advances, 11(4), eadr8243. https://doi.org/10.1126/sciadv.adr8243

95. Goldim, M. P. de S., Della Giustina, A., & Petronilho, F. (2019). Using evans blue dye to determine blood-brain barrier integrity in rodents. Current Protocols in Immunology, 126, e83. doi: 10.1002/cpim.83
96. Krueger, M., Bechmann, I., Immig, K., Reichenbach, A., Härtig, W., & Michalski, D. (2015). Blood-brain barrier breakdown involves four distinct stages of vascular damage in various models of experimental focal cerebral ischemia. Journal of cerebral blood flow and metabolism : official journal of the International Society of Cerebral Blood Flow and Metabolism, 35(2), 292–303. https://doi.org/10.1038/jcbfm.2014.199
97. Ferretti, M., Iulita, M.F., Cavedo, E. et al. Sex differences in Alzheimer disease — the gateway to precision medicine. Nat Rev Neurol 14, 457–469 (2018). https://doi.org/10.1038/s41582-018-0032-9
98. (2019). 2019 Alzheimer's disease facts and figures. *Alzheimer's & Dementia*, *15*(3), 321–387. https://doi.org/10.1016/j.jalz.2019.01.010
99. Dennison, J. L., Ricciardi, N. R., Lohse, I., Volmar, C. H., & Wahlestedt, C. (2021). Sexual Dimorphism in the 3xTg-AD Mouse Model and Its Impact on Pre-Clinical Research. Journal of Alzheimer's disease : JAD, 80(1), 41–52. https://doi.org/10.3233/JAD-201014
100. Hebda-Bauer EK, Simmons TA, Sugg A, Ural E, Stewart JA, Beals JL, Wei Q, Watson SJ, Akil H (2013) 3xTg-AD mice exhibit an activated central stress axis during early-stage pathology. J Alzheimers Dis 33, 407–422.
101. Stimmell AC, Baglietto-Vargas D, Moseley SC, Lapointe V, Thompson LM, LaFerla FM, McNaughton BL, Wilber AA (2019) Impaired spatial reorientation in the 3xTg-AD mouse model of Alzheimer's disease. Sci Rep 9, 1311.
102. Perez SE, He B, Muhammad N, Oh KJ, Fahnestock M, Ikonomovic MD, Mufson EJ (2011) Cholinotrophic basal forebrain system alterations in 3xTg-AD transgenic mice. Neurobiol Dis 41, 338–352.
103. Oh KJ, Perez SE, Lagalwar S, Vana L, Binder L, Mufson EJ (2010) Staging of Alzheimer's pathology in triple transgenic mice: A light and electron microscopic analysis. Int J Alzheimers Dis 2010, e780102

104. Yang JT, Wang ZJ, Cai HY, Yuan L, Hu MM, Wu MN, Qi JS (2018) Sex differences in neuropathology and cognitive behavior in APP/PS1/tau triple-transgenic mouse model of Alzheimer's disease. Neurosci Bull 34, 736–746.